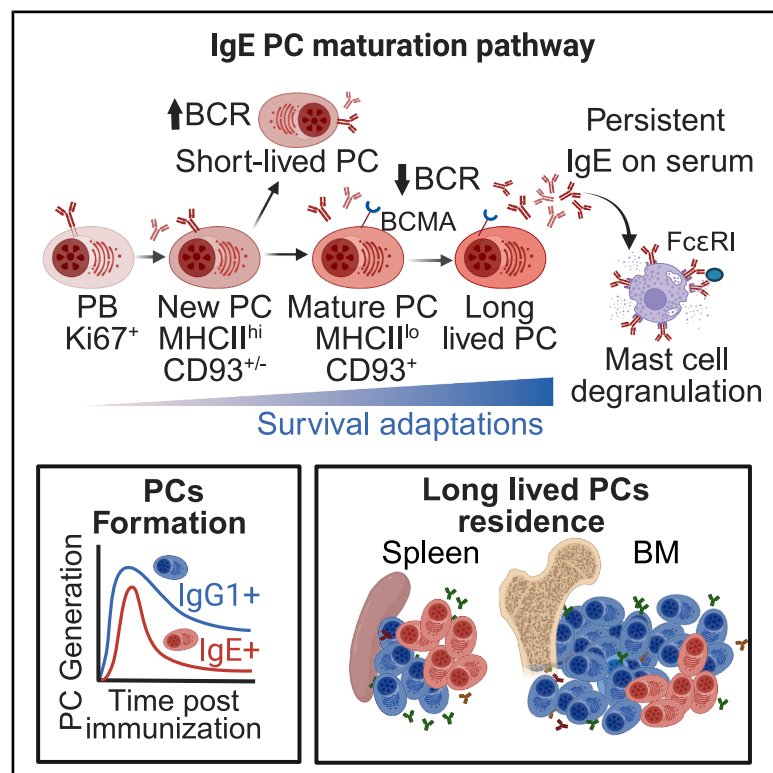


Immunity

Long-lived IgE plasma cells that reside in the spleen contribute to the persistence of the IgE response

Graphical abstract



Authors

Mariana C.G. Miranda-Waldetario,
Edgar Gonzalez-Kozlova,
Edenil C. Aguilar, ..., Emma S. Agudelo,
Jamie Redes,
Maria A. Curotto de Lafaille

Correspondence

mariana.waldetario@mssm.edu (M.C.G.
M.-W.),
maria.lafaille@mssm.edu (M.A.C.d.L.)

In brief

Allergies can persist even in the absence of allergen exposure. Miranda-Waldetario et al. find that IgE-producing plasma cells mature, acquire survival adaptations, and persist for extended periods of time in the spleen and bone marrow, secreting antibodies that can trigger anaphylaxis.

Highlights

- IgE PCs undergo maturation and become long-lived
- Mature IgE PCs downregulate the BCR and increase apoptosis resistance
- New IgE PC generation over time is severely reduced compared with IgG1 PCs
- Timestamping reveals that the spleen is a key reservoir of long-lived IgE PCs



Article

Long-lived IgE plasma cells that reside in the spleen contribute to the persistence of the IgE response

Mariana C.G. Miranda-Waldetario,^{1,2,3,*} Edgar Gonzalez-Kozlova,³ Ednenil C. Aguilar,^{1,2,3} Laura Xie,⁴ Kenneth B. Hoehn,⁵ Carlos J. Aranda,^{1,2} Yolanda Garcia-Carmona,^{1,2,3,6} Erica G.M. Ma,⁷ Emma S. Agudelo,^{1,2} Jamie Redes,^{1,2,3,8} and Maria A. Curotto de Lafaille^{1,2,3,9,10,*}

¹Precision Immunology Institute, Icahn School of Medicine at Mount Sinai (ISMMS), New York, NY 10029, USA

²Jaffe Food Allergy Institute, ISMMS, New York, NY 10029, USA

³Department of Immunology and Immunotherapy, ISMMS, New York, NY 10029, USA

⁴Department of Computational Biology, Weill Cornell Medicine, New York, NY 10065, USA

⁵Department of Biomedical Data Science, Geisel School of Medicine at Dartmouth, Hanover, NH 03755, USA

⁶MINDICH Child Health and Development Institute, ISMMS, New York, NY 10029, USA

⁷Department of Biochemistry & Molecular Pharmacology, New York University School of Medicine, New York, NY 10016, USA

⁸Graduate School of Biomedical Sciences, ISMMS, New York, NY 10029, USA

⁹Department of Pediatrics, ISMMS, New York, NY 10029, USA

¹⁰Lead contact

*Correspondence: mariana.waldetario@mssm.edu (M.C.G.M.-W.), maria.lafaille@mssm.edu (M.A.C.d.L.)

<https://doi.org/10.1016/j.immuni.2025.10.011>

SUMMARY

Expression of the IgE BCR is associated with increased B cell apoptosis, yet in persistent allergy, sustained production of IgE antibodies in the absence of allergen exposure suggests the existence of long-lived IgE plasma cells (PCs). Here we studied the development and localization of IgE PCs in mouse models of allergy. After immunization, IgE PCs underwent maturation in spleen and lymph nodes, acquiring a stable MHCII^{lo}CD93^{hi}CD98^{hi}BCR^{lo} phenotype. Mature IgE PCs had a distinct transcriptional profile adapted to high protein synthesis, glycosylation, and survival and resisted BCR-crosslinking-induced apoptosis. Immunization induced a burst of short-lived IgE PC formation, followed by a reduced differentiation rate over time, compared with IgG1 PCs. Timestamping of PCs revealed long-lived IgE PCs that localize to the spleen, in addition to the bone marrow (BM). Thus, immune challenge can generate both short-lived and long-lived IgE PCs, with long-lived IgE PCs in spleen and BM contributing to allergy persistence.

INTRODUCTION

High-affinity immunoglobulin E (IgE) antibodies mediate allergic diseases, owing to their ability to bind to cellular Fc ϵ RI receptors and induce mast cell degranulation upon crosslinking by allergens.¹ IgE antibodies production is highly restricted.^{2–4} IgE-expressing cells exist mainly as plasma cells (PCs),⁵ as IgE germinal center cells are transient and IgE memory B cells are scarce or nonexistent.^{6,7} The production of high-affinity IgE PCs in memory responses relies mainly on interleukin (IL)-4 receptor (IL-4R)-dependent sequential switching of type 2 IgG memory B cells.^{6,8–14}

IgE PCs are considered immature and short-lived. They have impaired response to the chemokine CXCL12¹⁵ and poor migration to the bone marrow (BM), rather remaining in lymphoid organs such as lymph nodes (LN) and spleen.^{5,7} Human IgE PCs from blood^{16,17} and from the nasal mucosa¹⁸ express higher MHCII than other PCs, suggesting an immature phenotype, as PC maturation involves reduced expression of MHCII.¹⁹ The decreased anaphylactic IgE response months after immunization in a mouse model of food allergy,²⁰ as well as the seasonal var-

iations of IgE antibodies to aeroallergens in allergic patients,²¹ argue for short lifetimes for IgE PCs. Furthermore, inhibition of IL-4R signaling in humans and mice, which prevents the generation of new IgE PCs, decreases circulating IgE^{22–24} and anaphylactic responses.²⁵

Membrane IgE (mIgE), the IgE B cell receptor (BCR), is a main driver of IgE cell fate. Forced mIgE expression induces PC differentiation^{26,27} and apoptosis via the Syk-BLNK-JNK/p38 pathway.²⁶ Chronic Ca²⁺ signaling by the IgE BCR contributes to cell death.²⁸ The cytoplasmic tail of mIgE promotes apoptosis by binding to Hax1.²⁹ Furthermore, crosslinking of the IgE BCR by anti-IgE antibodies or antigens can lead to IgE PC death.³⁰ This heightened predisposition to apoptosis supports the notion that IgE PCs are short-lived.

These findings stand in contrast to clinical observations supporting the existence of long-lived IgE PCs. In atopic individuals treated with blocking IL-4R antibodies, circulating IgE remains at about 40% of pre-treatment levels.^{22–24} IgE against food antigens persists in many allergic individuals avoiding the allergen.³¹ Individuals infected with filaria in an endemic area, retained parasite-specific IgE years after parasite clearance and moving to a



non-endemic country.³² In mice, IgE and IgG responses can persist up to 1 year after immunization, despite memory B cell depletion.³³ IgE PCs can persist in spleen and BM 100 days after the last antigen administration.³⁴ Repeated house dust mite administration generated long-lived BM IgE PCs detectable up to a year after immunization.³⁵ Multiple antigen exposures are usually necessary to develop high-affinity IgE antibodies^{5,35} and may also be required for development of long-lived IgE PCs.

Here we investigated the maturation, localization, and lifespan of IgE PCs in models of type 2 responses. We found that IgE plasmablasts swiftly undergo maturation into MHCII^{lo}CD93⁺ CD98^{hi}BCR^{lo} non-dividing PCs that acquire resistance to apoptosis and adaptation to high protein synthesis and glycosylation. Initially after immunization, IgE PCs were found preferentially in the LNs and spleen, and few were found in the BM, in contrast to IgG1 PCs that readily colonized the BM. At later times, 3–5 months after immunization, mature IgE PCs were similarly localized in spleen and BM, while mature IgG1 PCs were preferentially localized to the BM. Long-lived IgE PCs produced serum IgE antibodies able to mediate mast cell degranulation, demonstrating their functional role. Thus, IgE PCs progressively acquire features of longevity like other isotypes, and the spleen, in addition to the BM, is a main homing site of long-lived IgE PCs.

RESULTS

IgE PCs undergo maturation in secondary lymphoid organs and BM

To characterize IgE PC *in vivo*, we used TBmc mice, which have monospecific populations of CD4⁺ T and B cells recognizing chicken ovalbumin (OVA) and a linear peptide from influenza virus hemagglutinin, respectively.³⁶ TBmc mice develop augmented type 2 responses after immunization.^{5,36} To study antibody affinity maturation, TBmc mice are immunized with OVA cross-linked to a very low-affinity hemagglutinin mutant peptide (PEP1).^{5,36} Affinity maturation can then be tracked by the appearance of PEP1-specific antibodies and PEP1 affinity-enhancing mutations in the immunoglobulin genes.^{5,9}

To induce formation of IgE PCs, TBmc mice were immunized three times with OVA-PEP1 in alum. After 3 weeks, IgM-negative PCs from BM, mesenteric LNs (mLN), and spleen were sorted for to perform single-cell RNA sequencing (scRNA-seq) using the 5' 10x Genomics platform for whole-transcriptome and BCR analysis (Figure 1A). A total of 3,319 PCs with assembled BCRs were recovered across all tissues. Figure 1B shows the distribution of cells expressing IgGs, IgA, and IgE BCRs across tissues. IgG1 PCs were the most numerous, followed by IgE and IgA PCs and by lower numbers of IgG2a and IgG2b PCs. Very few IgG3 PCs were present in the dataset (not shown). IgG1 PCs were comparably distributed among BM, mLN, and spleen, while IgA, IgG2a, and IgG2c had similar distribution in spleen and BM but lower numbers in mLN. IgE PCs were distinctly distributed, being remarkably more numerous in spleen and mLN than in BM (Figures 1B and S1A).

Using Seurat analytical tool with exclusion of immunoglobulin genes, we identified 10 distinct transcriptional clusters (Figures 1C and S1B). The PC identity of cells in the clusters was confirmed by high expression of typical PC genes *Prdm1*, *Xbp1*, *Jchain*, and *Irf4* and low expression of typical naive/mem-

ory/germinal center B cell genes such as *Bach2* and *Bcl6* (Figures S1C and S1D).

To determine the differentiation status of PCs in the clusters, we analyzed differentially expressed genes (DEGs; Table S1). B cell differentiation into PCs involves upregulation of Blimp-1, which in turn negatively regulates the expression of MHCII genes.³⁷ New PCs emerge as dividing B220^{hi}MHCII^{hi} plasmablasts that further differentiate into non-dividing new PCs that undergo maturation into B220^{lo}MHCII^{lo} PCs, some of which became long-lived.³⁸ To identify plasmablasts, non-dividing new PCs, and mature PCs, we analyzed the expression of cell division-associated genes, *Mki67* and *Cdk1*, and the MHCII genes *H2-Aa*, *H2-Ab1*, and *H2-Eb1* (Figure 1D). Cluster 8 had high expression of *Mki67* and other cell division genes as well as MHCII genes and thus contained plasmablasts. Clusters 4 and 5, which contained non-dividing PCs with high MHCII expression, were identified as recently formed “new” PCs. All other clusters, 0, 1, 2, 3, 6, 7, and 9, which contained non-dividing PCs with low expression of MHCII genes, were classified as mature PCs. Other DEGs of plasmablasts and new PC clusters included *Bsg* and *Mzb1*, while *Cst3* was differentially expressed in all mature clusters, and *Junb* and *Nikbia* were differentially expressed in mature clusters 0, 1, 2, 3, and 6 (Figure 1D; Table S1).

Some clusters had a dominant isotype composition. For example, cluster 1 had predominantly IgA PCs, and cluster 3 had predominantly IgE PCs, while other clusters contained multiple isotypes (Figure 1E). BM PCs were mostly found in clusters of mature PCs—0, 1, 6, and 7—whereas PCs from spleen were found in all clusters, and mLN PCs were more frequent in clusters 2, 3, 4, 5, and 8 (Figure 1F). IgE PCs were present in early clusters 8, 4, and 5 and in the mature clusters 3 and 6. Few IgE PCs were also found in clusters 7 and 9. BM IgG1 PCs were predominantly found in cluster 0 followed by cluster 7, and BM IgA PCs were mostly found in clusters 1 and 7 (Figures 1E and S1A). In this analysis, new IgA PCs were scarce in BM, mLN, and spleen, as most of the IgA PCs were in mature cell clusters.

DEGs for each cluster were identified and are shown in Table S1 and Figure S1E. Clusters 4, 5 (new PCs), and 8 (plasmablasts) shared higher expression of several genes including *Mzb1* and *H-2* genes. Cluster 5 was closer to cluster 8 than cluster 4, suggesting that cluster 5 contain PCs of an earlier maturation stage than cluster 4. Cluster 0 was characterized among other genes by expression of *Lyc1* and *Lyc2*. Cluster 6 had the highest expression of *Itgb7* and *Tnsfr17* (encoding BCMA). Top DEGs of cluster 1 included genes previously linked to IgA PCs such as *Runx2*, *Klf2*, and *Ccr10*.^{39–41} *Klf2* was also differentially expressed in clusters 3 and 6, which contain mature IgE PCs.

The analysis of somatic hypermutation (SHM) frequency and of high-affinity mutations^{5,9,11} (Figures 1G–I, S1F, and S1G) revealed that plasmablasts (cluster 8) and new PCs of cluster 5 had the highest SHM frequency, and clusters 0 and 9, followed by 1 and 7 (all mature PC), had the lowest frequency of SHM. On the other hand, new PC clusters 4 and 5 had the lowest frequency of high-affinity mutations, while mature clusters 0, 7, and 9 had the highest frequency of high-affinity mutations (Figure 1H). Consistently, the ratio of high-affinity mutations to SHM was highest for mature clusters 0, 7, and 9 and lowest for new clusters 4 and 5 (Figure 1I). Thus, new PCs appeared to have been formed from

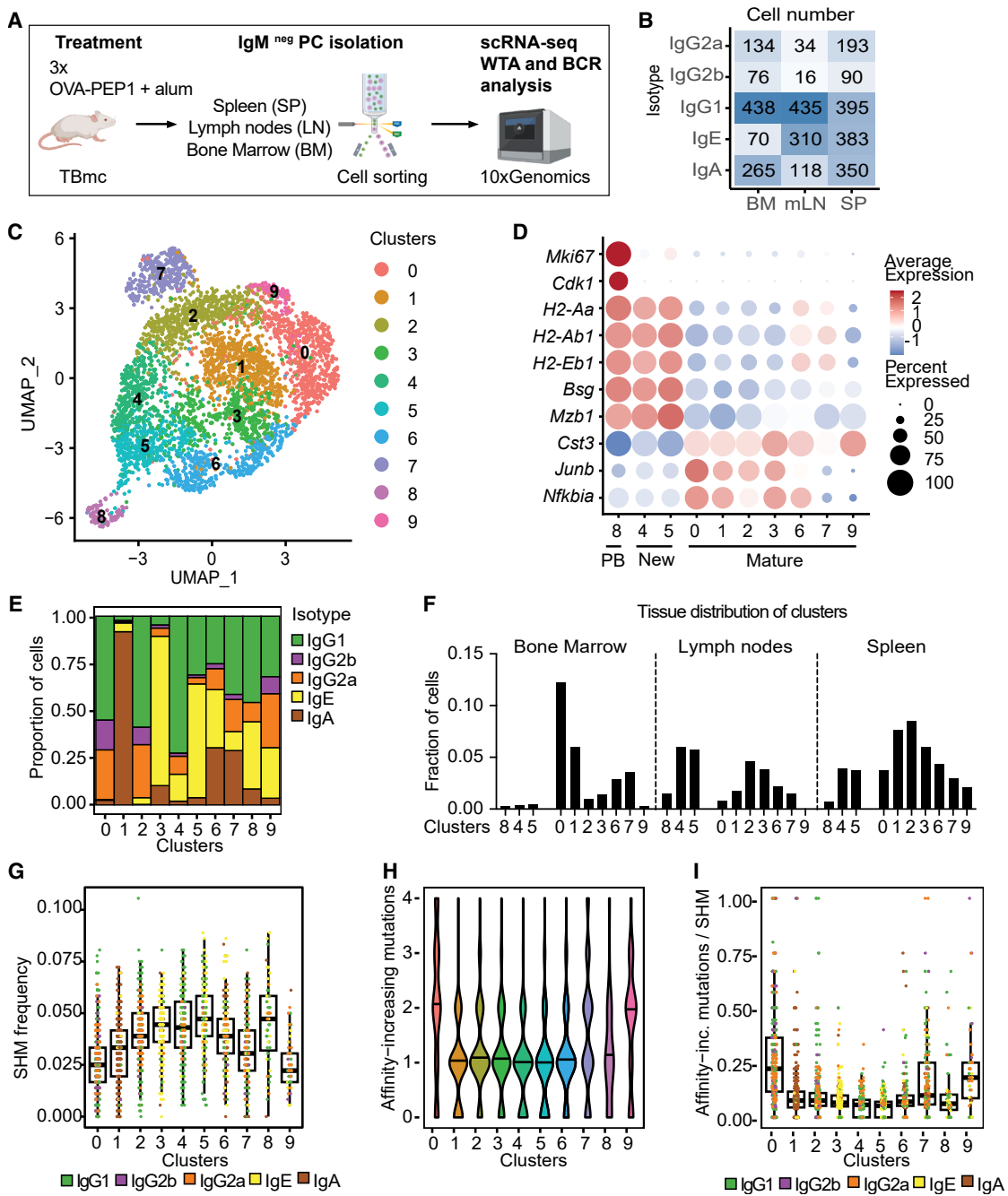


Figure 1. Transcriptional analysis of PCs of immunized mice

- (A) Workflow of scRNA-seq analysis. IgM⁻CD138⁺CD98⁺ PCs were isolated from the spleen (SP), mesenteric lymph nodes (LN), and BM of 3-times immunized TBmc mice, at 3 weeks after the last immunization.
- (B) Total number of sequenced cells per isotype and organ.
- (C) UMAP of PC clusters after Seurat analysis.
- (D) Dot plots of selected genes to identify plasmablasts (PB), new PCs, and mature PCs.
- (E) Proportion of PCs expressing switched isotypes per cluster.
- (F) Distribution of cells per cluster in BM, LN, and spleen.
- (G) Frequency of SHM per cluster, colored by isotype.
- (H) Violin plots: distribution of BCRs carrying 0–4 high-affinity mutations in their CDR3 heavy chain, per cluster.
- (I) Ratio of high-affinity mutation frequency to SHM frequency per cluster.

See also Figure S1.

highly mutated lower-affinity clones, while mature PC contained less mutated higher-affinity clones.

In terms of isotype, IgE PCs had the highest levels of SHM, followed by IgG1 PCs (Figure S1F). However, the IgG1 PC population contained more cells with two to four high-affinity mutations per sequence than the IgE PC population (Figure S1G), as we observed before.¹¹

In sum, we identified new and mature PCs in a mouse model of multiple immunizations. Maturation of the PC response was characterized by exit from the cell cycle and decreased expression of MHCII. IgE PC underwent maturation, but mature IgE PCs at this time of analysis (3 weeks after last immunization) were preferentially found in spleen and mLN rather than in the BM.

IgE PCs have increased expression of genes of ER stress, protein synthesis, and glycosylation

To identify transcriptional differences between IgE and IgG1 PCs, we grouped the PCs of each of these isotypes contained in new or mature PC clusters. Plasmablasts were excluded as their transcriptional profile was dominated by cell division genes. Spleen and mLN PCs of each isotype were grouped, as they were found in overlapping regions of the uniform manifold approximation and projection (UMAP) (Figure S1B). UMAP of tissue specific, new, and mature IgE and IgG1 PCs are shown in Figure 2A. Spleen + mLN contained new and mature IgE and IgG1 PCs, while BM contained mostly mature PCs of both isotypes (Figure 2A). We then compared IgE and IgG1 PCs from the following groups: new PCs from spleen + mLN (SP+LN), mature PCs from spleen + mLN, and mature PCs from BM (Figure 2B; Table S2). Overall, differences between IgE and IgG1 PCs involved higher expression of many genes in IgE PCs, compared with IgG1 PCs. Among the genes with higher expression in IgE PCs were *Slc3a2*, encoding for the amino acid transporter CD98; *Fcer2*, encoding for the IgE low-affinity receptor CD23; and *IL-13Ra*. In addition, new IgE PCs displayed higher expression of *Rgs1*, a regulator of G protein signaling and CXCL12-mediated migration.⁴²

In both isotypes, there was a tendency toward decreased expression of many genes along maturation in spleen + mLN. Mature IgE PCs had a distinct transcriptional profile including higher expression of some genes exclusively in this population (Figure 2B; Table S2). Genes highly expressed in IgE PCs compared with IgG1 PCs included those of the endoplasmic reticulum (ER) stress and unfolded protein response (UPR) (Figure 2C), protein synthesis, and N-glycosylation (Figure 2D). Nevertheless, these pathways tended to attenuate during maturation in both isotypes (Figures 2C and 2D). Consistently, using the ModuleScore function, we found that the ER stress score was highest in new IgE and IgG1 PCs from spleen + mLN cells and lowest in mature PCs of spleen + mLN and BM (Figure 2E). The translation score was also higher in new versus mature IgE PCs of spleen + mLN and BM and in new versus mature IgG1 PCs of spleen + mLN (Figure 2F). The N-glycosylation score was highest in IgE than IgG1 PCs and decreased with maturation in both isotypes (Figure 2G). This adaptation of IgE PCs may respond to the high N-glycosylation demand for IgE antibodies.⁴³

Consistently, with the higher translation score, we found that when cultured in the presence of APRIL and IL-6,⁴⁴ IgE PCs

secreted more antibodies on a per cell basis than IgG1 PCs (Figures S2A–S2F).

In agreement with the maturation patterns of clusters, pseudo-time analysis of IgE and IgG1 PCs (Figures S3A–S3C) revealed a negative correlation between high pseudotime score and expression of ER stress genes (Figure S3B). Furthermore, in the clusters' analysis, the overall ER stress score was higher in plasmablasts and new PC clusters (clusters 8, 5, and 4) than in mature PC clusters (Figure S3C). To validate these findings in a polyclonal lymphocyte model, we performed bulk RNA-seq of IgE and IgG1 PCs isolated from spleen and mLN 8 days after a secondary infection with *Nippostrongylus brasiliensis* (*N. brasiliensis*) (Figures S3D–S3F). Polyclonal IgE PCs displayed overall higher expression of genes related to ER stress response (Figure S3E), protein synthesis, and N-glycosylation pathways (Figure S3F), compared with IgG1 PCs. Overall, the results indicate that even though cellular stress and protein synthesis pathways are attenuated as IgE PCs mature, these pathways remain more elevated in IgE PCs than IgG1 PCs.

Mature IgE PCs upregulate expression of survival genes

To assess the potential for long-term persistence of mature IgE PCs, we analyzed the expression of genes associated with PC survival and lifespan. We found that mature IgE PCs of spleen + mLN and of BM expressed higher levels of survival genes *Tnfrsf17* (encoding BCMA), *Tnfrsf13b* (encoding TACI), and *JunB*, as well as a set of genes (*Pim1*, *Gpx4*, and *Lars2*) known to promote cell survival under cellular stress (Figure 3A),^{45–47} than new IgE PCs.

Compared with other PCs, mature BM IgE PCs expressed elevated levels of *Bcl2* and *Mcl1*, critical anti-apoptotic genes.⁴⁸ *CD93*, encoding C1qr1, a protein required for maintenance of antibody secretion in PC,⁴⁹ was also highly expressed in BM IgE PCs (Figure 3A). IgE PCs from cluster 6 had the highest expression of survival genes (Figure S4A). Projection of IgE PCs expressing *Bcl2* and *Mcl1* in the UMAP demonstrated the localization of *Bcl2*⁺ IgE PCs in mature clusters 6 and 3 (Figure 3B), while *Mcl1*⁺ IgE PCs were more broadly distributed (Figure 3C). Expression of some survival genes (e.g., *Tnfrsf17* and *Tnfrsf13b*) was higher in mature IgE PCs than mature IgG1 PCs, which suggests that different PC isotypes rely on different survival strategies.

We previously described that circulating IgE PCs isolated from asthma and atopic dermatitis patients differentially express *Atf5*,¹⁶ an ER stress response gene associated with secretory cell survival,⁵⁰ and *Laptm5*, a negative regulator of BCR expression and B cell activation.⁵¹ *Laptm5* was highly expressed by mature BM IgE PCs (Figure 3A). Polyclonal IgE PCs isolated early after secondary *N. brasiliensis* infection also displayed higher expression of *Atf5*, *Laptm5*, *Bcl2*, and *Tnfrsf17* (Figure S4B). We next compared the transcriptional profile of murine mature IgE PCs from our scRNA-seq dataset with that of human IgE PCs isolated from BM.^{52,53} To identify commonly upregulated genes, we intersected our list of mature IgE PCs DEGs with the sets of enriched genes reported in both studies. We found 145 common DEGs of higher expression in our dataset and in Pacheco et al.,⁵³ 62 common to our dataset and Vecchione et al.,⁵² and 61 common DEGs of higher expression across all three datasets (Figure S4C; Table S3). Among those we found

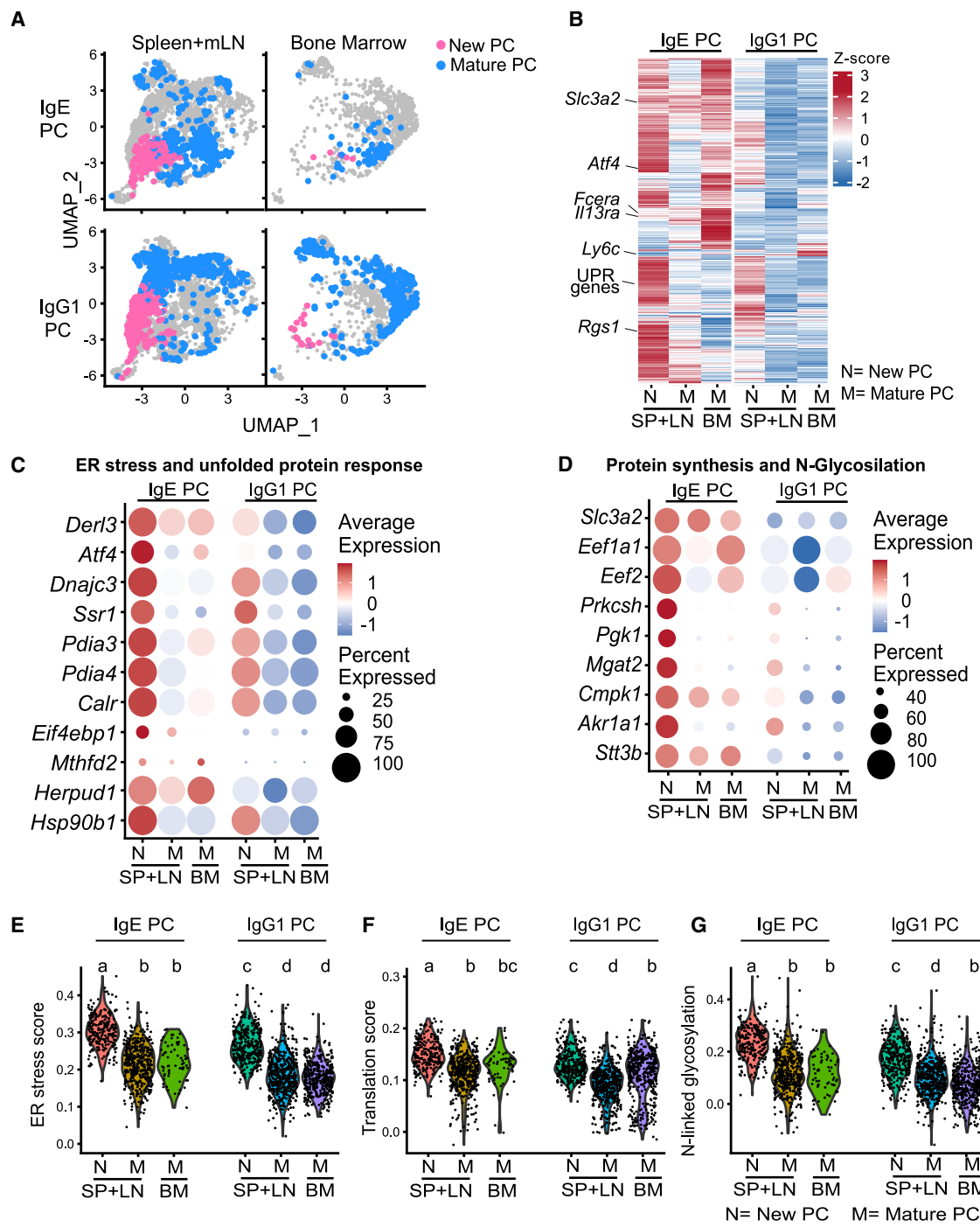


Figure 2. IgE PCs' transcriptional profile denotes distinct adaptation to the secretory function

(A) UMAP projection of new and mature IgE and IgG1 PCs from spleen + mLN and from BM.

(B) Heatmap of DEGs ($p \leq 0.05$) between new (N) and mature (M) IgE and IgG1 PCs from spleen and mLN (SP + LN) and mature (M) IgE and IgG1 PCs from BM. UPR, unfolded protein response.

(C and D) Dot plots of selected genes associated with the ER stress and UPR (C) and with protein synthesis and N-glycosylation (D).

(E–G) Violin plots showing gene signature scores for ER stress (E), translation score (F), and N-linked glycosylation (G). Statistical analysis was performed using one-way ANOVA. Groups labeled with different letters are significantly different (adjusted $p < 0.05$, Tukey's multiple comparisons test).

See also Figures S2 and S3.

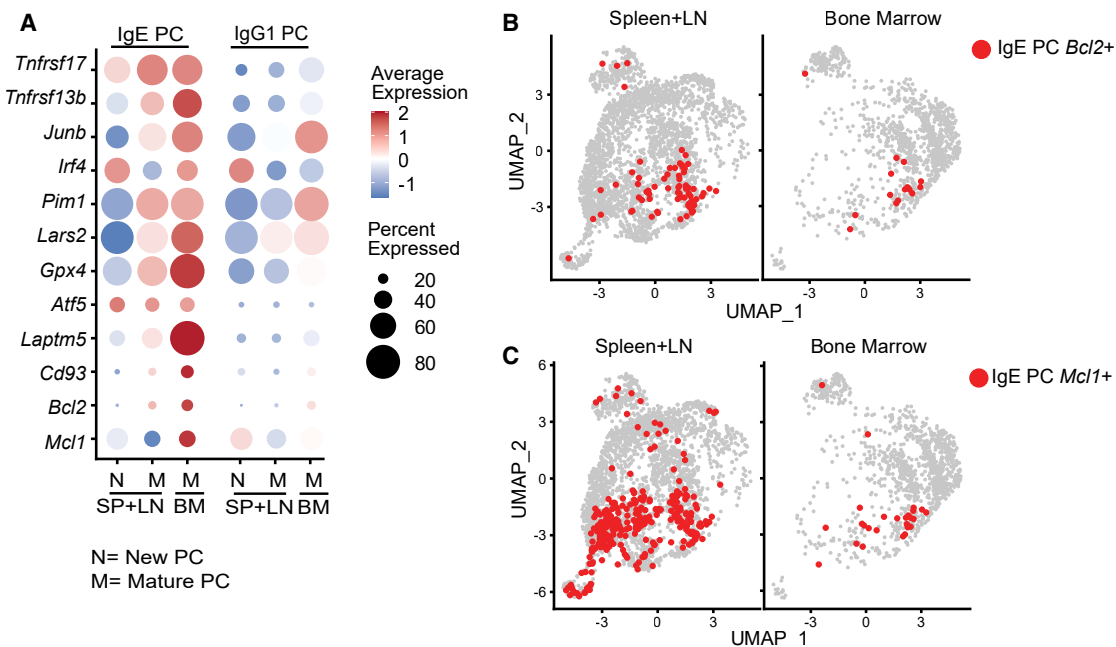


Figure 3. Cell survival signatures of mature IgE PCs

(A) Dot plots of relative expression of selected genes associated with PC survival in new (N) and mature (M) IgE and IgG1 PCs from spleen and mLN (SP + LN) and mature (M) IgE and IgG1 PCs from BM.

(B and C) UMAP projections of *Bcl2*⁺ (B) and *Mcl1*⁺ (C) IgE PCs from spleen+mLN (left) and from BM (right).

See also Figure S4.

survival-related genes such as *TNFRSF17*, *ATF5*, and *BCL2*; the amino acid transporter *SLC3A2*; and genes associated with ER stress response, protein synthesis, and N-linked glycosylation (e.g., *MTHFD2*, *EEF1A1*, and *CMPK1*). The comparative analysis across mouse and human datasets further supports the conservation of this signature in mature IgE PCs across species. In sum, we demonstrated that the maturation of IgE PCs involves increased expression of genes important for PC survival.

Dynamics of IgE PC localization in spleen and BM after a primary immunization

To better understand the kinetics of IgE PC formation and persistence, we analyzed PCs from spleen and BM of TBmc mice over 150 days after primary immunization (Figure 4A). Total IgG1 and IgE antibody levels increased after immunization. While IgG1 antibodies remained elevated by day 150, IgE levels decreased after day 70, following immunization (Figure 4B). As previously described,⁵ circulating PEP1-specific IgE antibodies were detected later than PEP1-specific IgG1 antibodies, and the PEP1-specific IgE titers, which peaked on day 70, were about 10-fold lower than those of IgG1 (Figure 4C).

IgE and IgG1 PCs in spleen and BM were analyzed by flow cytometry (Figures S5A and 4D). Splenic PCs peaked at days 16–30 and decreased thereafter (Figure S5B). As expected, BM PCs increased later, peaking by day 100 after immunization (Figure S5C), consistent with PC formation in secondary lymphoid organs followed by migration to the BM.⁵⁴ PCs frequency was very low in unimmunized TBmc mice but increased over time in spleen and BM (days 0 and 100, PBS) (Figures S5B and S5C).

We next determined the frequency of spleen and BM IgE and IgG1 PCs along the 150 days post-immunization (Figures 4D–4F). IgE and IgG1 PCs were undetectable in spleen and BM of most unimmunized mice on day 0 (Figures 4E, 4F, S5D, and S5E). IgG1 PC frequency was highest at day 16 of immunization, in spleen, and decreased thereafter (Figure 4E).

Consistent with the IgE antibody response, IgE PCs peaked between days 30 and 70 in spleen, when they constituted about 40% of all splenic PCs, in contrast to IgG1 PCs that, at this point, represented about 40% of BM PCs (Figure 4F). After 70 days, IgE PC frequency decreased to about 20% in the spleen at day 100 and remained at similar level until day 150 post-immunization (Figure 4E). On the other hand, IgG1 PC frequency remained stable in the BM. There was delayed accumulation of IgE PCs in the BM, remaining at constant frequency from day 70 to day 150 post-immunization (Figure 4F).

To determine if new IgE PCs formation accounted for their accumulation in the spleen, we analyzed the kinetics of Ki-67 expression after immunization (Figures 4G and 4H). The highest percentages of Ki-67⁺ IgG1 and IgE PCs were observed at day 16 of immunization when at least half of both PC isotypes expressed Ki-67 (Figures 4G and 4H). Ki-67⁺ IgE PCs decreased drastically by day 30 post-immunization to about 1% by day 150. By contrast, 30% or more of IgG1 PCs in spleen were Ki-67⁺ up to day 100 post-immunization, suggesting a higher rate of IgG1 PC generation past the peak and over a prolonged period. To corroborate the difference in IgE PC and IgG1 PC generation at later times after immunization, we administered BrdU in the drinking water from days 56 to 70 post-immunization. After 14 days, an average of 9% IgE PCs cells and of 36% of IgG1 PCs

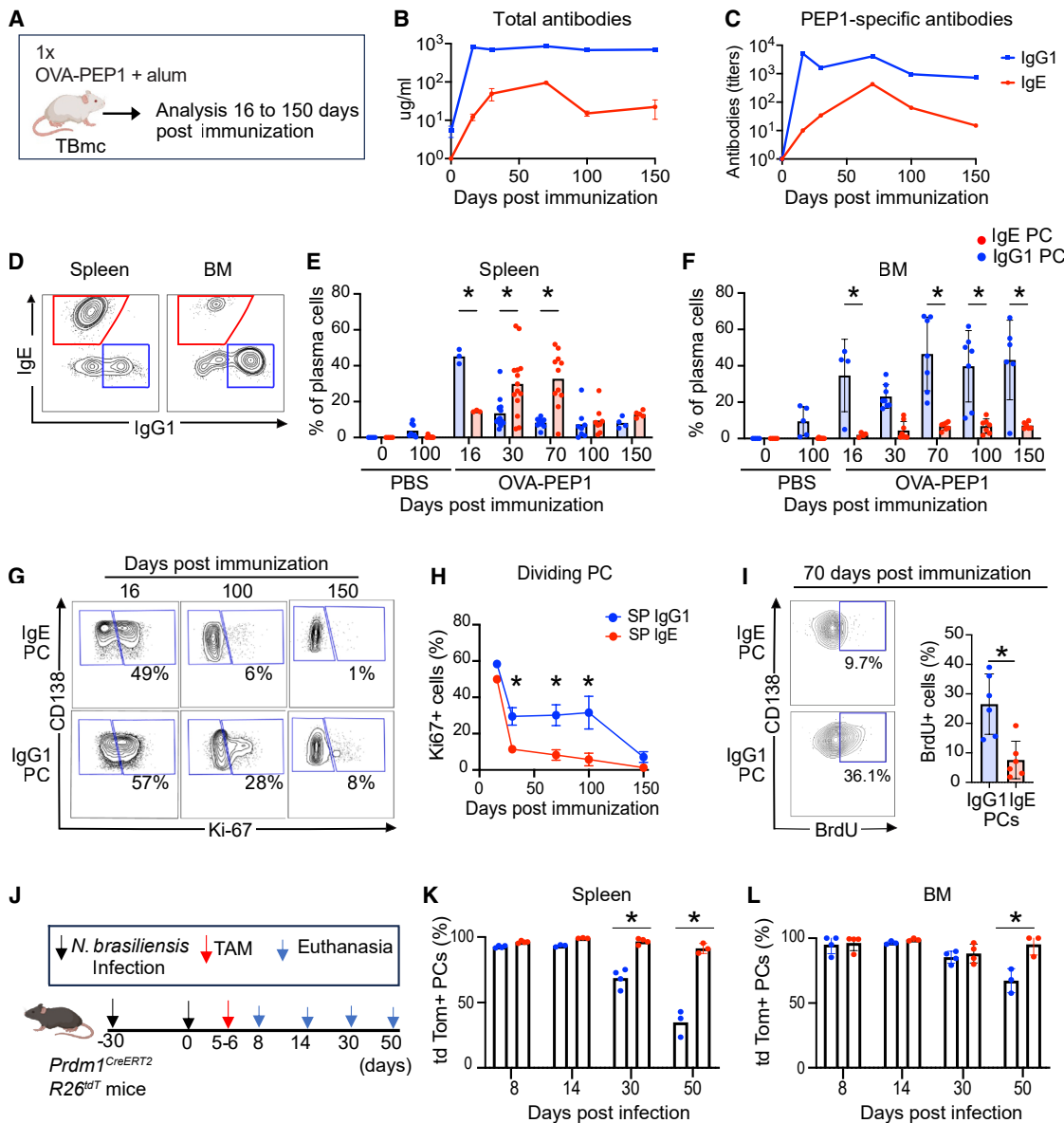


Figure 4. Kinetics of formation and maturation of IgE PCs

(A) Experimental design for (B)–(H). TBmc mice were immunized once by intraperitoneal injection with OVA-PEP1 in alum. PCs and antibodies were analyzed from days 16 to 150 after immunization.

(B and C) Total (B) and PEP1-specific (C) IgE and IgG1 antibodies in plasma ($n = 3\text{--}4$ mice per time point).

(D) Representative plots of IgE and IgG1 PCs 70 days post-immunization. Plots contain gated CD138⁺CD98⁺IgA⁻IgM⁻ PCs.

(E and F) Percentages of IgE and IgG1 PCs among spleen PCs (E) and BM PCs (F). Data were aggregated from three independent experiments. Each dot corresponds to one mouse sample.

(G and H) Ki-67 staining of IgE and IgG1 PCs at 16, 100, and 150 days post-immunization. Representative contour plots (G) and quantification (H). Data were from two combined experiments ($n = 3\text{--}5$ mice per time point).

(I) BrdU incorporation by IgE and IgG1 PCs on day 70 post-immunization. Data are from two combined experiments ($n = 6$ mice).

(J) Experimental design for (K) and (L). *Prdm1*^{CreERT2}*R26*^{rt} mice were infected subcutaneously with *N. brasiliensis* on days 30 and 0 and administered tamoxifen (TAM) on days 5 and 6 to timestamp PCs. PCs were analyzed on days 8, 14, 28, and 50 post-secondary infection.

(K and L) Percentage of tdTomato⁺ among IgE and IgG1 PCs in the spleen (K) and BM (L). $n = 3\text{--}4$ mice per time point.

In (B), (C), (E), (F), (H), (I), (K), and (L), mean \pm SEM are shown. Statistical analysis was performed using unpaired Student's *t* test (*: $p \leq 0.05$).

See also Figures S5 and S6.

were BrdU⁺ (Figure 4I). This higher generation of IgG1 PCs without splenic accumulation, together with their sustained BM numbers, suggests that a swift migration of new IgG1 PCs to the BM maintains the IgG1 PC BM population. By contrast, the reduced formation of new IgE PCs, together with their accumulation in the spleen and limited BM localization, suggests distinct homeostatic turnover rates between the two isotypes in the spleen and BM.

We then used the *Prdm1*^{CreERT2}*R26*^{tdT} mouse strain generated in our laboratory (Figure S6A), which allows for timestamping of nearly all PCs at a chosen time by administering tamoxifen (Figures S6B–S6D). PC frequency post-immunization was comparable in *Prdm1*^{CreERT2}*R26*^{tdT} and wild-type mice (Figure S6B). Following tamoxifen, ~98% of existing PCs in the spleen and BM expressed dtTomato (Figure S6C and S6D), while new PCs formed after tamoxifen would be dtTomato⁻. We observed an average of 2% of dtTomato⁺ germinal center B cells and less than 1% dtTomato⁺ memory B cells (Figure S6E). There was very low spontaneous Cre-recombinase activity in PCs of *Prdm1*^{CreERT2}*R26*^{tdT} mice that did not receive tamoxifen (Figure S6F). Using this model, we analyzed PC differentiation responses in mice with polyclonal T and B lymphocyte repertoires.

Prdm1^{CreERT2}*R26*^{tdT} mice were infected with the parasite *N. brasiliensis*, which induces transient IgG1 and IgE PC responses.⁶ *Prdm1*^{CreERT2}*R26*^{tdT} mice were on a C57Bl/6 genetic background that is less prone to type 2 and IgE responses.⁵⁵ To increase the number of PCs, we analyzed PCs after a secondary infection. Tamoxifen was administered on days 5 and 6 post-re-infection, and PCs were analyzed on days 8, 14, 30, and 50 thereafter (Figure 4I). In this model, spleen IgE PCs were less abundant than spleen IgG1 PCs at all time points analyzed, except at day 30 post-immunization (Figure S6H). Very few IgE PCs were observed in the BM after infection (Figure S6J). As anticipated, IgE PCs were less abundant and did not persist for as long as observed in the TBmc model. At day 8 post-infection, more than 95% of all spleen and BM IgG1 and IgE PCs were tdTomato⁺ (Figures 4K–4L), allowing us to track the PC turnover in both isotypes. The percentage of tdTomato⁺ IgG1 PCs in spleen declined to about 70% on day 30 and to less than 40% on day 50, reflecting the formation of new, tdTomato⁻ IgG1 PCs (Figures 4K and S6G). By contrast, IgE PCs that remained up to day 50 post-infection were more than 90% tdTomato⁺ and were mostly found in the spleen (Figures S6G–S6J), suggesting low or no IgE PC formation at the late time points in this model. IgG1 turnover was observed in the BM but to a lesser extent than in the spleen. Furthermore, 60% of the IgG1 BM were tdTomato⁺ 50 days after infection (Figures 4L and S6I). This experiment supports the notion that IgE PCs form at a lower rate than IgG1 PCs at later times after immunization.

Together, these results indicate that IgE and IgG1 PCs differ in their spatial distribution and formation dynamics. IgE PCs are generated early in larger numbers following immunization or infection, but their formation declines over time, and their migration to the BM is limited. By contrast, IgG1 PCs continue to be generated at higher rates even at later stages post-immunization and efficiently populate the BM. Furthermore, the data indicate that the spleen and BM are key sites of long-term IgE PC localization.

Mature MHCII^{lo}CD93⁺ IgE PCs are detected long after immunization in the spleen

The kinetics of the appearance of early, mature, and long-lived spleen IgE PCs after primary immunization was analyzed at various time points after immunization using spectral cytometry. Cells were stained to determine PC identity (CD138 and CD98), maturation state (Ki-67 and MHCII), isotype (IgM, IgA, IgG1, and IgE), and the expression of other described PC proteins,^{56,57} or proteins identified in our scRNA-seq analysis (Table S1). tSNE-CUDA was used to identify populations within the PC gate at 16 and 100 days after primary immunization (Figure S7A). Isotype-specific PCs were identified through manual gating and projected in the UMAP clusters of samples from day 16 and 100 after immunization (Figure 5A). UMAP revealed little overlap between day 16 and day 100 PCs, indicating phenotypic shifts over time (Figure 5A). Each isotype occupied a defined region in the combined 16 + 100 days tSNE map (Figures 5B and S7B). Ki-67⁺MHCII^{hi} cells were characterized as plasmablasts, and Ki-67⁻MHCII^{hi} cells were characterized as early PCs. Plasmablasts and early PCs were found among IgM⁺, IgG1⁺, and IgE⁺ PCs.

Two areas of IgE PCs were clearly distinguished in the tSNE plots, one corresponding to plasmablasts and early PCs, which predominated at day 16, and the other corresponding to mature PCs, which predominated at day 100 (Figure 5A). CD93 was consistently expressed in MHCII^{lo} PCs of all isotypes (Figure 5B), indicating its association with maturation of PCs. However, CD93 was also expressed in some early PCs; therefore, additional markers, such as MHCII, were necessary to refine the identification of mature PCs.

To map the dynamics of maturation in IgE and IgG1 PCs, we evaluated the changes in expression of MHCII and CD93 in splenic PCs over 150 days following immunization. These two markers identified three distinct PC subpopulations: MHCII^{hi} CD93⁺, MHCII^{hi}CD93⁻, and MHCII^{lo}CD93⁺ (Figure 5C). At 16 days post-immunization most IgE and IgG1 PCs expressed MHCII, as expected for early PC,³⁸ and part of the MHCII^{hi} PC populations expressed CD93 (Figures 5C–5E). Over time, MHCII^{lo}CD93⁺ PCs emerged, presumably by downregulation of MHCII in MHCII^{hi}CD93⁺ PCs. By day 150, most IgE PCs were MHCII^{lo}CD93⁺. Ki-67 expression was highest in MHCII^{hi}CD93⁻ PC, followed by MHCII^{hi}CD93⁺, and was mostly absent in MHCII^{lo}CD93⁺ PCs, confirming the mature status of the latter (Figure 5F). A large part of MHCII^{hi}CD93⁻ and MHCII^{hi} CD93⁺ IgG1 PCs were dividing cells (Ki-67⁺) (Figure 5H), while fewer IgE PCs were Ki-67⁺ in these populations (Figure 5G).

Other differences were observed between IgE and IgG1 PCs (Figures S7C–S7G). Unlike IgG1 PCs, mature IgE PCs did not express EpCAM or Ly6C (Figures S7C–S7E). IgE PCs expressed higher levels of CD98 than IgG1 PCs, and part of the IgE PCs population expressed CD23, unlike IgG1 PCs (Figures S7F and S7G).

This analysis demonstrated that as a population, IgE PCs exit cell division and progressively acquire a more mature phenotype with a faster kinetics than IgG1 PCs. This is consistent with reduced IgE PC formation after peak response versus a sustained IgG1 PCs formation as evidenced by the sizable population of MHCII^{hi}Ki-67⁺ IgG1 PCs even after 70 days post-immunization (Figure 5E).

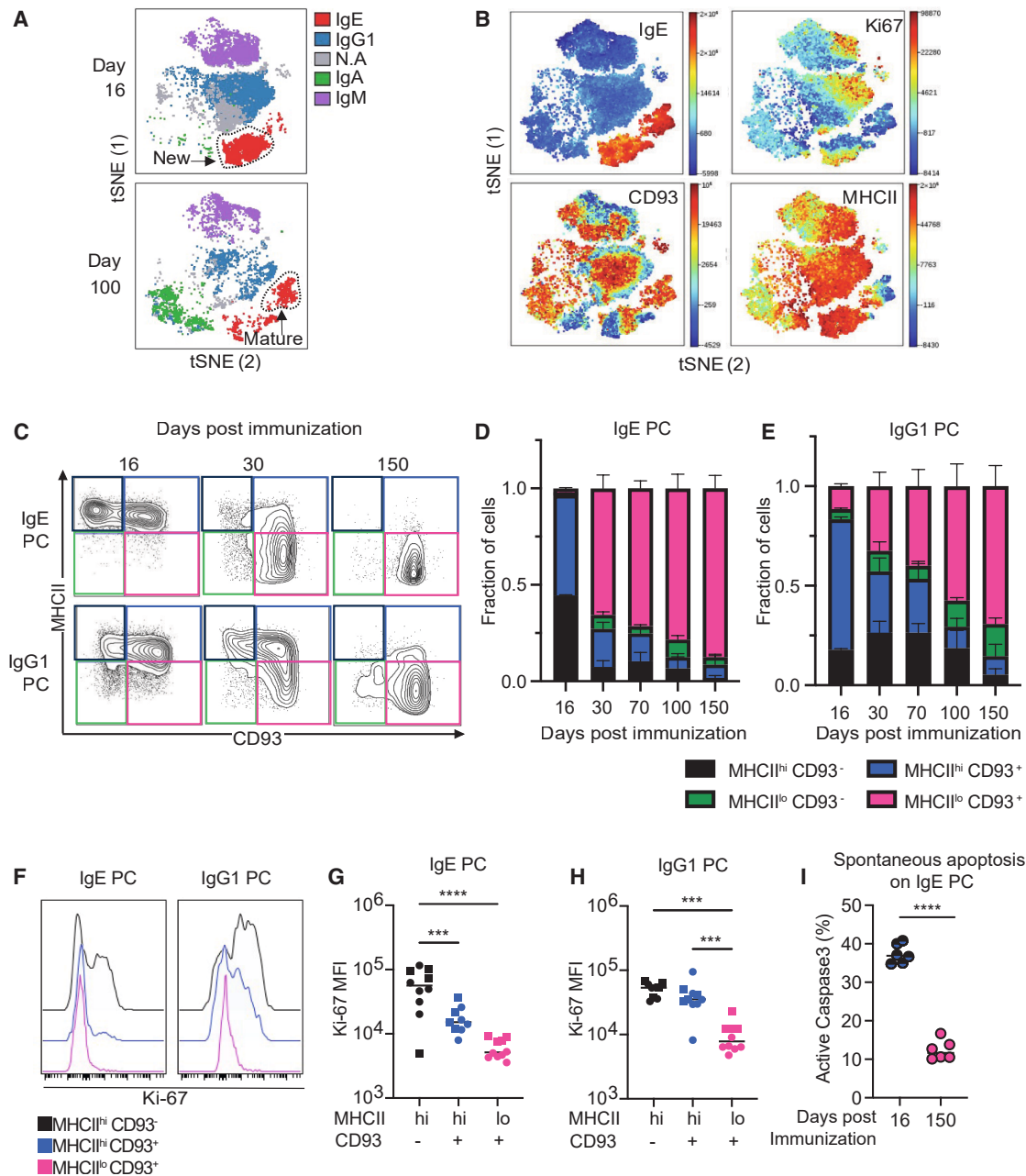


Figure 5. Mature IgE PCs are MHCII^{lo}CD93⁺CD98⁺

(A) Projection of PC isotypes on concatenated tSNE plots of spleen PCs from TBmc mice at 16 or 100 days post-immunization. New and mature IgE PCs are indicated.

(B) tSNE plots showing expression of IgE, Ki67, CD93, and MHCII in concatenated samples of PCs from 16 and 100 days post-immunization.

(C) Representative plots of the expression of MHCII and CD93 in gated IgE PCs (upper row) or IgG1 PC (lower row) at 16, 30, and 150 days post-immunization.

(D and E) Changes in IgE (D) and IgG1 (E) PC subpopulations over 150 days after immunization. Data are from two combined experiments. $n = 3\text{--}6$ mice.

(F) Representative histograms of Ki-67 expression in MHCII^{hi}CD93⁻, MHCII^{hi}CD93⁺, and MHCII^{lo}CD93⁺ subpopulations of splenic IgE and IgG1 PCs. Data are from concatenated samples of days 30 and 150 after immunization.

(G and H) Ki-67 mean fluorescence values in subpopulations of IgE (G) and IgG1 (H) PCs. Each symbol represents one mouse (squares: day 30; circles: day 150). Statistical significance is indicated by **** $p \leq 0.0001$.

(I) Ex vivo spontaneous apoptosis of IgE PCs from 16 and 150 days post-immunization, evaluated by caspase-3 activity. Each dot represents a well. $n = 8\text{--}9$ mice per immunization time.

In (D), (E), and (G)–(I), mean \pm SEM are shown. In (G)–(I), statistical analysis was performed using one-way ANOVA for (G) and (H) and Student's *t* test for (I).

** $p \leq 0.01$, *** $p \leq 0.001$, **** $p \leq 0.0001$.

See also Figure S7.

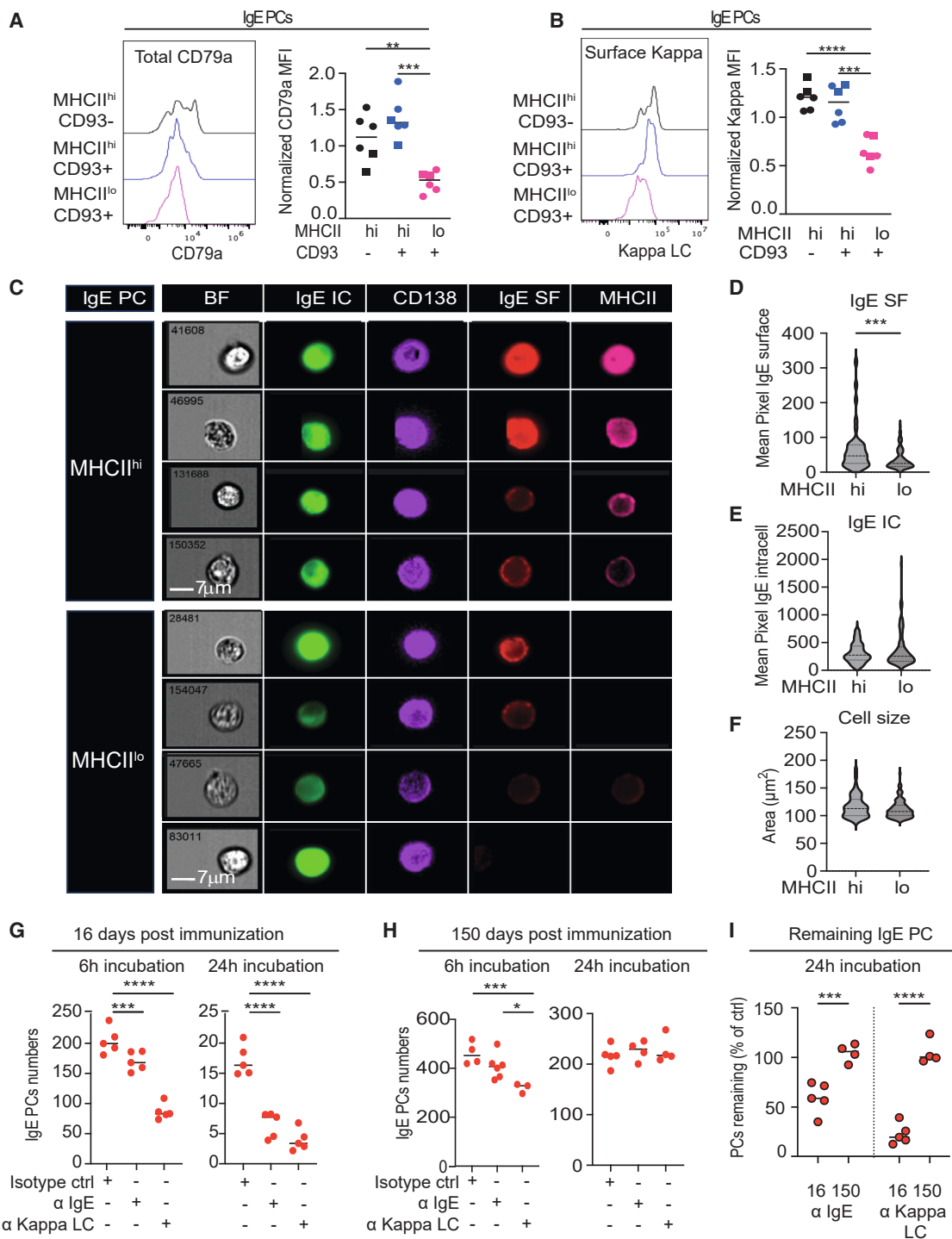


Figure 6. Mature IgE PCs downregulate membrane IgE

(A and B) CD79a (A) and surface kappa LC (B) expression in splenic IgE PCs. Representative histograms are shown on the left. MFI values normalized to the MHCII^{hi}CD93⁺ population are shown on the right. Squares and circles indicate samples from mice at days 30 and 150 post-immunization, respectively. $n = 6$ mice from two independent experiments.

(C) Representative images of the expression of surface IgE (SF, red) and MHCII (pink) in IgE PCs identified by co-expression of CD138 (purple) and intracellular IgE (IC, green). Images were captured by AMNIS image flow cytometry. Scale bar, 7 μm .

(D–F) Violin plots of the quantification of cell area (D), intracellular IgE fluorescence intensity (E), and surface IgE fluorescence intensity (F) in 150 individual IgE PC images gated as MHCII^{hi} or MHCII^{lo}.

(legend continued on next page)

To evaluate the dynamics of maturation and persistence of IgE PCs in an additional allergy model, we analyzed PCs in a model of peanut food allergy. Peanut sensitization was induced in *Il4raF709* mice⁵⁸ by intragastric administration of peanut butter with staphylococcal enterotoxin B (SEB) (Figure S7H). IgE, IgG1, and IgA PCs from mLN, spleen, and BM were quantified 130 days after the final gavage (Figure S7I). At this late time point, IgG1 PCs were predominantly localized in the BM, while IgE PCs were similarly distributed in spleen and BM (Figure S7I). IgA PC numbers were also comparable in spleen and BM.

Mature MHCII^{lo} IgE PCs were detected in both mLN and spleen (Figure S7J); however, approximately 30% of IgE PCs in mLN and 20% in spleen expressed MHCII, indicating a higher degree of ongoing IgE PC formation at this stage in this model, compared with the TBmc model. Nonetheless, the proportion of new IgE PCs was still lower than that observed for IgG1 PCs (74% MHCII^{hi}IgG1 PCs in mLN and 30% in spleen) and IgA PCs (77% MHCII^{hi}IgA PCs in mLN and 40% in spleen) (Figure S7K). These findings demonstrate the persistence of IgE PCs in another immunization model and reinforces their distinct pattern of maturation and tissue localization.

We then asked if maturation protected IgE PCs from apoptosis. We tested the spontaneous apoptosis of early and mature IgE and IgG1 PCs from spleen at 16 and 150 days post-immunization (Figure 5I). Total spleen cells were incubated at 37°C for 6 h and then analyzed for caspase-3 activity. Only about 10% of all IgE PCs from 150 days post-immunization were apoptotic, compared with about 35% of IgE PCs from 16 days post-immunization. These results are consistent with the findings of the transcriptional analysis showing that maturation of IgE PCs is associated with increased expression of cell survival and apoptosis resistance genes.

Mature IgE PCs have lower membrane BCR expression and became resistant to BCR-signaling-induced cell death

To determine if downregulation of mlgE occurs during PC maturation, we evaluated the expression of CD79a, a signaling component of the BCR, and the surface expression of kappa light chain (LC) among the differentiating IgE PCs (Figures 6A, 6B, and S8A). Both CD79a and surface kappa LC were lower in mature MHCII^{lo}CD93⁺ IgE PCs than in MHCII^{hi} subsets. In addition, ImageStream flow cytometer, showed that MHCII^{hi} IgE PCs expressed significantly higher levels of mlgE than MHCII low/negative cells (Figure 6D). Cell size and intracellular IgE were comparable between populations (Figures 6E and 6F). These findings indicate that IgE PCs downregulate mlgE expression during maturation.

We next tested whether BCR downregulation in mature IgE PCs confer resistance to BCR-induced cell death.³⁰ Spleen cells were isolated at 16 or 150 days after immunization and incubated *ex vivo* with anti-IgE or anti-kappa LC antibodies to induce BCR crosslinking (Figures 6G–6I). Quantification of IgE PCs at 6 and

24 h post-treatment showed a significant reduction in IgE PC numbers, following both anti-IgE and anti-kappa treatments, in 16-day-post-immunization PCs, compared with isotype control treatment (Figure 6G). By contrast, 150 days post-immunization, IgE PCs showed reduced sensitivity to BCR engagement; only a minor yet significant decrease in cell number was observed 6 h after anti-kappa treatment, while no significant loss was detected after anti-IgE treatment (Figure 6H). At 24 h, the proportion of 150-day IgE PCs remaining was similar between anti-IgE-, anti-kappa-, and isotype-treated samples, suggesting that mature IgE PCs are much more resistant to BCR-induced apoptosis than newly formed IgE PCs. Mature IgE PCs also resisted higher anti-IgE doses (Figure S8B).

To assess *in vivo* the sensitivity of mature IgE PCs to BCR-mediated elimination, we fate-mapped PCs in *Prdm1*^{CreERT2}*R26*^{tdT} mice and subsequently challenged the mice with anti-IgE antibody treatment (Figures S8C–S8E). Consistent with the *ex vivo* data, the tdTomato negative IgE PC frequency was reduced after anti-IgE administration, compared with isotype-treated controls, indicating higher sensitivity of new IgE PCs to BCR crosslinking (Figure S8D and S8E). These findings support the notion that mature IgE PCs acquire resistance to BCR-mediated depletion.

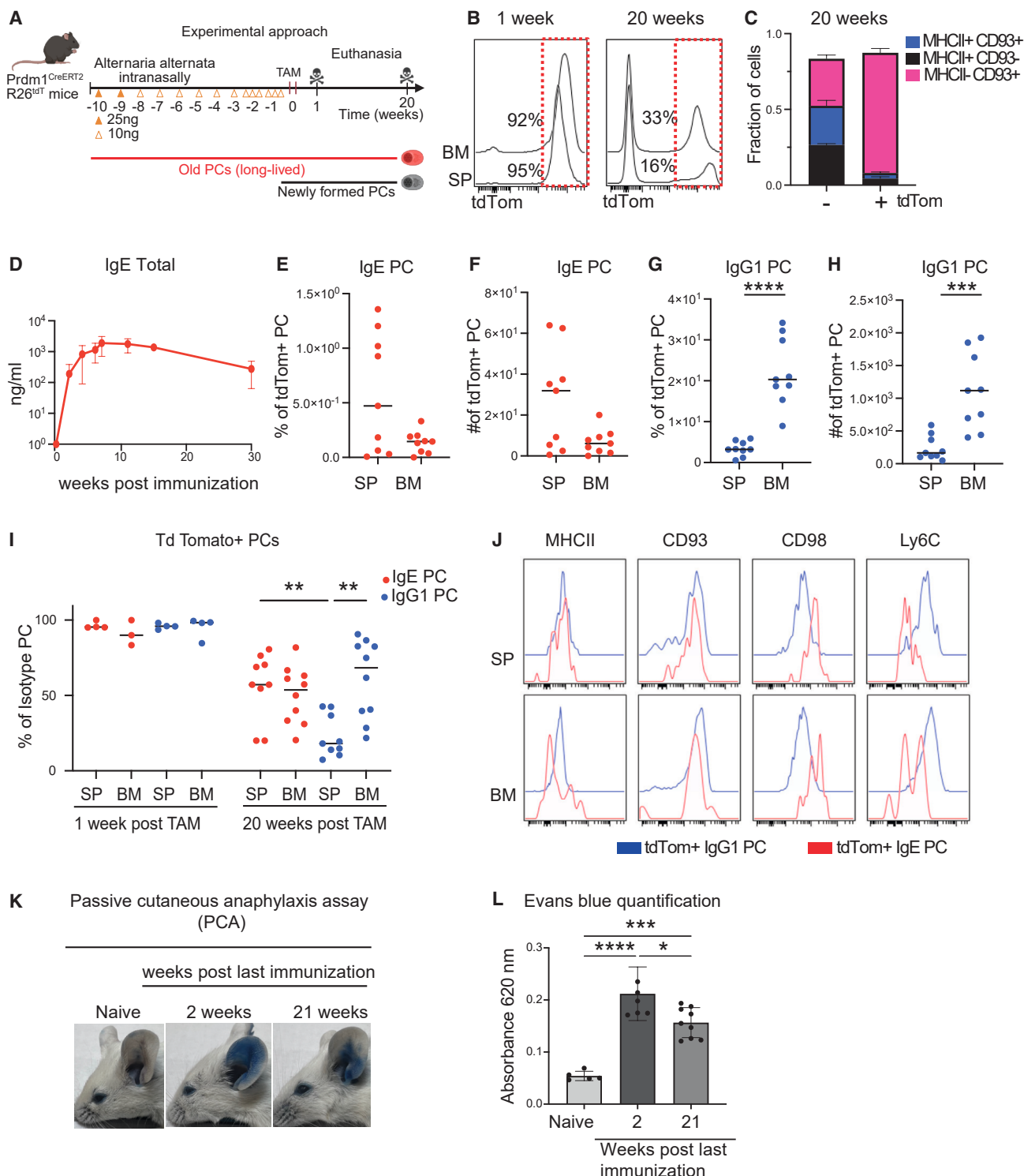
Long-lived IgE PCs have a mature phenotype

To more accurately assess the persistence of IgE PC, we timestamped and followed IgE PCs in a model of allergic airway disease induced by *Alternaria alternata*.⁵⁹ *Alternaria alternata* extract was administered to *Prdm1*^{CreERT2}*R26*^{tdT} by intranasal route over a 10-week period. At the end of the immunization, PCs were labeled by administration of tamoxifen (Figure 7A). After 1 and 20 weeks, we evaluated the phenotype of PCs in spleen and BM (Figures 7B, 7C, and S9). Notably, 1 week after tamoxifen administration, 92% of BM PCs and 95% of spleen PCs were tdTomato⁺, confirming the efficiency of the PC timestamping method (Figure 7B). Over time, a higher turnover of PCs was observed in the spleen compared with the BM; after 20 weeks, only 16% of spleen PCs remained tdTomato⁺, whereas about 30% of BM PCs remained tdTomato⁺ (Figure 7B). At week 20, the tdTomato⁻ fraction was a mix of PCs aged between 1 day and 20 weeks and contained new and mature PCs populations (MHCII^{hi}CD93⁻, MHCII^{hi}CD93⁺, and MHCII^{lo}CD93⁺). On the other hand, the 20-week-old tdTomato⁺ fraction was formed by mature MHCII^{lo}CD93⁺ PCs (Figure 7C). Plasma IgE peaked at week 8 and decreased thereafter, persisting at higher levels than baseline at the 30-week time point (Figure 7D). Persistence of IgE antibodies in the plasma was associated with the persistence of tdTomato⁺ IgE PCs in spleen and BM (Figures 7E and 7F). We observed significant variation on IgE PC frequency between mice, and the observed differences between spleen and BM did not reach statistical significance. By contrast, there was preferential localization of tdTomato⁺ IgG1 PCs in the BM compared with spleen (Figures 7G and 7H). As observed

(G and H) Total splenocytes were isolated at days 16 (G) or 150 (H) post-immunization and incubated for 6 or 24 h with anti-IgE (αlgE), anti-kappa light chain (αKappa LC), or isotype control for 6 or 24 h to assess BCR crosslinking-induced apoptosis.

(I) Percentage of IgE PCs remaining after 24 h, normalized to isotype control. $n = 8\text{--}9$ mice. Each dot represents one well.

Statistical analysis was performed using unpaired Student's *t* test for (D)–(F) and one-way ANOVA for all other panels. * $p \leq 0.05$, ** $p \leq 0.01$, *** $p \leq 0.0001$. See also Figure S8.

**Figure 7. Timestamping reveals mature phenotype of long-lived IgE PCs**

(A) Experimental design for (B)–(L). *Prdm1*^{CreERT2}*R26*^{tdt} mice were chronically exposed to intranasal *Alternaria alternata* extract for 10 weeks followed by 2 gavages of tamoxifen (TAM) on alternating days. PCs were analyzed at 1 and 20 weeks post-tamoxifen.

(B) Frequency of tdTomato⁺ PCs in the spleen (SP) and BM at 1 and 20 weeks post-tamoxifen.

(C) Distribution of MHCII^{hi}CD93⁻, MHCII^{hi}CD93⁺, and MHCII^{lo}CD93⁺ PC subpopulations among tdTomato⁻ and tdTomato⁺ PCs at 20 weeks post-tamoxifen. *n* = 9 mice.

(D) Plasma levels of total IgE. *n* = 9 mice.

(legend continued on next page)

previously in the *N. brasiliensis* infection model (Figure 4K), formation of new PCs in the spleen was higher among IgG1 PCs than IgE PCs. Only about 14% of splenic IgG1 PCs remained tdTomato⁺, contrasting with 60% of tdTomato⁺ IgE PCs (Figure 7I). On the other hand, the relatively high proportion of tdTomato⁻ IgE PCs indicated a higher late IgE PC formation in this model, compared with the *N. brasiliensis* infection model.

No significant differences in the proportion of tdTomato⁺ IgE PCs were observed between IgE PCs in the spleen and BM (Figure 7I), indicating that while the BM is a well-established niche for IgG1 PC persistence, the spleen and BM are sites for the long-term maintenance of IgE PCs.

We confirmed that long-lived tdTomato⁺ IgG1 and IgE PCs in the spleen and BM displayed the MHCII^{lo}CD93⁺ mature phenotype. Furthermore, long-lived IgE PCs expressed high levels of CD98 and low levels of Ly6C (Figure 7J), as described for long-lived IgE PCs in the TBmc model (Figures S7D and S7E).

Finally, we evaluated the physiological function of persistent IgE PCs. We performed a passive cutaneous anaphylaxis (PCA) assay using plasma from 2- and 21-weeks after the last antigen administration in the *Alternaria* model, corresponding to 1- and 20-weeks post-tamoxifen (Figure 7A). As expected, an anaphylactic reaction was observed when 1-week-post-tamoxifen plasma was injected, as measured by blue dye extravasation in the ear (Figures 7K and 7L). Notably, IgE antibodies from >20 weeks post last immunization were also able to induce anaphylaxis (Figures 7K and 7L). These results indicate that long-lived IgE PCs are functionally relevant and contribute to the allergic response.

DISCUSSION

We found that a subset of IgE PCs formed in response to immunization can undergo maturation within secondary lymphoid organs and become long-lived, thereby challenging the paradigm that IgE PCs are immature and short-lived. Long-lived IgE PCs produce IgE antibodies that mediate anaphylaxis, thus contributing to the persistence of allergic responses. Contrary to the notion that IgE PCs in secondary lymphoid organs are immature, our data revealed that the spleen, in addition to the BM, is a key site of long-lived IgE PC persistence.

Mature IgE PCs expressed genes common to mature PCs of other isotypes, such as *Cst3*, *Junb*, and *Nfkbia*, and genes involved in PC survival, such as *Bcl2*, *Mcl1*, *Tnfrsf17* (encoding BCMA),⁶⁰ *Tnfrsf13b* (encoding TACI), *Pim1*,⁶¹ *Lars2*,⁴⁷ and *Gpx4*.⁴⁶ TACI and BCMA are receptors for BAFF and APRIL, important survival cytokines secreted by stroma cells in the BM^{62,63} and by dendritic cells and macrophages in secondary

lymphoid organs.⁶⁴ This transcriptional adaptation was associated with the acquisition by IgE PCs of resistance to spontaneous and BCR crosslinking-induced apoptosis.

While following general principle of PC maturation, IgE PCs have distinct adaptations to antibody secretion and to survival. The expression of ER stress and translation pathways was augmented in IgE PCs, compared with IgG1 PCs, as recently described.⁵² IgE antibodies are highly N-glycosylated,⁴³ and glycosylation is linked to IgE pathogenesis.^{65,66} Consistently, the expression of N-glycosylation genes was higher in IgE PCs than IgG1 PCs.

IgE PCs differentially expressed *Atf5*, an ER stress response gene⁵⁰; *Laptm5*, encoding a transmembrane lysosomal protein controlling membrane BCR expression and B cell activation⁵¹; *Rgs1*, an inhibitor of chemokine receptor signaling⁴²; *Fcer2*, encoding the low-affinity IgE receptor CD23; and *IL13ra*. *Atf5*, *Laptm5*, and *Fcer2* also have higher expression in circulating human IgE PCs¹⁶ and human BM IgE PCs^{52,53} than in other PCs.

The significance of the expression of *Fcer2* and *IL13ra* in IgE PCs is not yet known, but higher expression of *IL13ra* has also been observed in transcriptomic analysis of long-lived PCs.⁵⁷ Expression of *Fcer2* and *IL13ra* in IgE PCs could be a consequence of the ontogeny of these cells, as IgG memory B cells expressing *Fcer2* and other IL-4R-regulated genes have recently been found to be the likely precursors of IgE PCs in persistent allergy.^{12,13,16} Increased expression of *Rgs1* in IgE PCs may be in part responsible for their deficient response to CXCL12¹⁵ and deficient localization to the BM. CXCR4, the receptor for CXCL12, is necessary for the long-term homing of PCs to the BM.⁶⁷ Despite their deficient response to CXCL12,¹⁵ the levels of CXCR4 in IgE PCs are comparable to those of IgG1 PCs.⁵²

PCs decrease production of membrane immunoglobulin while highly increasing the synthesis of the secreted form of immunoglobulin (antibody), a process regulated by differential mRNA polyadenylation and splicing.⁶⁸ Murine IgE PCs formed at the peak of a primary response express higher levels of mlgE than IgE germinal center cells, contrary to the decrease in mlgG1 in differentiating IgG1 PCs.^{6,7} In this study, we found that maturation of IgE PCs involved decreased production of mlgE. These differences may be due to transcriptional or splicing regulation and/or to the increase in *Laptm5* expression, which may promote lysosomal degradation of the IgE BCR.

The lifespan of IgE PCs has been a topic of active debate. In a model of food allergy, the half-life of the IgE PC population was calculated to be 60 days, while IgG1 PC half-life was estimated to be 234 days.²⁰ We found that in the TBmc model, IgE PCs numbers were high in the spleen until 70 days post-immunization, then they decreased, but small numbers of IgE PCs

(E–H) Quantification of tdTomato⁺ IgE and IgG1 PCs at 20 weeks post-tamoxifen. (E and F) Frequency (E) and absolute number per 10⁶ tissue cells (F) of tdTomato⁺ IgE PCs in SP and BM. (G and H) Frequency (G) and absolute number per 10⁶ tissue cells (H) of tdTomato⁺ IgG1 PCs in SP and BM.

(I) Percentage of tdTomato⁺ cells among IgE and IgG1 PCs, at 1 and 20 weeks post-tamoxifen.

(J) Expression of MHCII, CD93, CD98, and Ly6C in tdTomato⁺ IgE and IgG1 PCs from SP and BM at 20 weeks post-tamoxifen.

(K and L) PCA assay. IgG-depleted plasma from naive mice or from immunized mice at 1 or 20 weeks post-tamoxifen was injected into the ears of naive recipients. After 24 h, mice were challenged intravenously with *Alternaria alternata* extract plus Evan's Blue dye. (K) Representative pictures showing the extravasation of blue dye. (L) Quantification of dye vascular leakage in the ear. Each dot represents one mouse ear.

Statistical analysis of (E)–(H) was done using Mann-Whitney U test and all others using one-way ANOVA; *p ≤ 0.05, **p ≤ 0.01, ***p ≤ 0.0001. Data are shown as mean ± SEM.

See also Figure S9.

persisted in spleen and BM up to the final analysis 150 days post-immunization. After the early peak of short-lived PCs, there was much reduced IgE PC generation, reflecting a low turnover, and their localization in spleen and BM indicated a distinct tissue distribution pattern. By contrast, IgG1 PCs were generated at higher rates past the early peak and efficiently migrate to the BM, contributing to a stable population through ongoing turnover and long-time persistence.

We observed higher late-stage IgE PC formation in the food allergy and asthma models, compared with the TBmc immunization model and the *N. brasiliensis* infection model. This suggests that the type of immunization and route of antigen exposure may influence the dynamics of IgE PC generation and persistence.

The current models of long-lived PC development support a continuum of differentiation, in which only a small subset of PCs gradually acquire the molecular and functional properties required for long-term survival.^{38,57,69–71} Long-lived PC differentiation entails increased expression of survival genes and progressive acquisition of a sustained stable phenotype associated to low MHCII and CD93 expression.^{38,57,71} This subset typically emerges as a continuum throughout the immune response, with peak of formation during the late germinal center.^{69,70} Our findings indicate that IgE PCs follow this general model of progressive maturation, but with isotype-intrinsic characteristics that influence their generation and migratory behavior. Specifically, their restricted access to BM niches may constrain their accumulation in classical long-lived compartments, while allowing a subset to persist in the spleen.

The studies of IgE PC biology described here demonstrate that IgE PCs undergo maturation and terminal differentiation through the acquisition of an expression program that, while sharing features common to other PCs, displays distinct adaptations to cellular stress and survival. Using timestamping of PCs, we demonstrated the existence of long-lived IgE PCs and the spleen as an important niche of long-lived IgE PC persistence. Our findings have implications for understanding the mechanisms involved in persistent human allergy and for developing cell-targeting therapies in allergy.

Limitations of the study

Our study provides direct evidence that IgE PCs can mature and persist within the spleen in murine models of allergy. The extent to which human secondary lymphoid organs harbor long-lived IgE PCs was not investigated here and is still unknown. Therefore, our findings cannot be directly generalized to human IgE responses.

Kinetically, we determined that IgG1 PCs are generated over a longer period than IgE PCs after immunization, but the mechanisms involved were not determined. We did not investigate if long-lived IgE PCs of the spleen would be displaced by new PCs forming in responses to unrelated antigens; thus, the long-term stability of IgE PCs in face of immune challenges is not known.

To enrich for switched PCs in the scRNA-seq analysis, we exclude IgM PCs, and since our study focused on IgG1 and IgE PCs, other IgG and IgA PCs were not analyzed in depth. This prevented comparisons of tissue localization and lifespan of all PCs.

RESOURCE AVAILABILITY

Lead contact

Further information and requests for resources and reagents should be directed to and will be fulfilled by the lead contact, Maria A. Curotto de Lafaille (maria.lafaille@mssm.edu).

Materials availability

All unique materials generated in this study are available from the [lead contact](#) with a completed materials transfer agreement.

Data and code availability

Bulk RNA-seq data have been deposited in NCBI under BioProject: PRJNA1289849. scRNA-seq data have been deposited under BioProject: PRJNA1200005.

ACKNOWLEDGMENTS

We thank Pedro Silva, Ankita Prakash, and Jeffrey Adames for mouse colony and general laboratory support; the Human Immuno Monitoring Center and the Genomics and Flow Cytometry Cores at ISMMS for technical support; and Juan Lafaille and members of the M.A.C.d.L. laboratory for critical reading of the manuscript. Cartoons were created using BioRender. Work in the M.A.C.d.L. laboratory was supported by NIH grants R01AI130343, R01AI151707, and R01AI153708 and by a grant from the Job Research Foundation.

AUTHOR CONTRIBUTIONS

M.C.G.M.-W. and M.A.C.d.L. conceptualized the study and designed the experiments. M.C.G.M.W. carried out the experiments and performed analysis. E.C.A. and E.S.A. helped with experiments. E.G.-K. and L.X. performed the computational analysis. K.B.H. performed BCR analysis. C.J.A. generated the *Prdm1*^{creERT2} mice. Y.G.-C. helped with the AMINIS experiment. E.G.M. M. performed the initial experiments leading to the project. J.R. set up the food allergy model. M.C.G.M.-W. and M.A.C.d.L. wrote the manuscript. M. A.C.d.L. supervised the project. All authors read and approved the manuscript.

DECLARATION OF INTERESTS

The authors declare no competing interests.

STAR METHODS

Detailed methods are provided in the online version of this paper and include the following:

- [KEY RESOURCES TABLE](#)
- [EXPERIMENTAL MODEL AND STUDY PARTICIPANT DETAILS](#)
 - Mouse strains
 - Immunizations and infections
 - BrdU incorporation
 - Tamoxifen treatment
- [METHOD DETAILS](#)
 - ELISA
 - Preparation of OVA-PEP1 crosslinked antigen
 - IgG antibody depletion from plasma
 - Flow cytometry
 - Quantification of surface and intracellular IgE
 - BCR crosslinking assay on mature IgE plasma cells
 - Passive cutaneous anaphylaxis assay
 - Antibody secretion assay
 - Bulk RNAseq
 - 10X Genomics scRNaseq
 - Single cell gene expression analysis
 - Functional scoring and pathway analysis
 - Analysis comparison across species
 - B cell receptor sequence processing and analysis
- [QUANTIFICATION AND STATISTICAL ANALYSIS](#)

SUPPLEMENTAL INFORMATION

Supplemental information can be found online at <https://doi.org/10.1016/j.immuni.2025.10.011>.

Received: December 20, 2024

Revised: June 20, 2025

Accepted: October 8, 2025

Published: October 31, 2025

REFERENCES

1. Galli, S.J., and Tsai, M. (2012). IgE and mast cells in allergic disease. *Nat. Med.* 18, 693–704. <https://doi.org/10.1038/nm.2755>.
2. Saunders, S.P., Ma, E.G.M., Aranda, C.J., and Curotto de Lafaille, M.A. (2019). Non-classical B Cell Memory of Allergic IgE Responses. *Front. Immunol.* 10, 715. <https://doi.org/10.3389/fimmu.2019.00715>.
3. He, J.S., Narayanan, S., Subramaniam, S., Ho, W.Q., Lafaille, J.J., and Curotto de Lafaille, M.A. (2015). Biology of IgE production: IgE cell differentiation and the memory of IgE responses. *Curr. Top. Microbiol. Immunol.* 388, 1–19. https://doi.org/10.1007/978-3-319-13725-4_1.
4. Wade-Vallance, A.K., and Allen, C.D.C. (2021). Intrinsic and extrinsic regulation of IgE B cell responses. *Curr. Opin. Immunol.* 72, 221–229. <https://doi.org/10.1016/j.coim.2021.06.005>.
5. Erazo, A., Kutchukhidze, N., Leung, M., Christ, A.P.G., Urban, J.F., Jr., Curotto de Lafaille, M.A., and Lafaille, J.J. (2007). Unique maturation program of the IgE response in vivo. *Immunity* 26, 191–203. <https://doi.org/10.1016/j.immuni.2006.12.006>.
6. He, J.S., Meyer-Hermann, M., Xiangying, D., Zuan, L.Y., Jones, L.A., Ramakrishna, L., de Vries, V.C., Dolpady, J., Aina, H., Joseph, S., et al. (2013). The distinctive germinal center phase of IgE+ B lymphocytes limits their contribution to the classical memory response. *J. Exp. Med.* 210, 2755–2771. <https://doi.org/10.1084/jem.20131539>.
7. Yang, Z., Sullivan, B.M., and Allen, C.D.C. (2012). Fluorescent in vivo detection reveals that IgE(+) B cells are restrained by an intrinsic cell fate predisposition. *Immunity* 36, 857–872. <https://doi.org/10.1016/j.immuni.2012.02.009>.
8. Fernandes-Braga, W., and Curotto de Lafaille, M.A. (2024). B cell memory of Immunoglobulin E (IgE) antibody responses in allergy. *Curr. Opin. Immunol.* 91, 102488. <https://doi.org/10.1016/j.coim.2024.102488>.
9. Xiong, H., Dolpady, J., Wabl, M., Curotto de Lafaille, M.A., and Lafaille, J.J. (2012). Sequential class switching is required for the generation of high affinity IgE antibodies. *J. Exp. Med.* 209, 353–364. <https://doi.org/10.1084/jem.20111941>.
10. Turqueti-Neves, A., Otte, M., Schwartz, C., Schmitt, M.E.R., Lindner, C., Pabst, O., Yu, P., and Voehringer, D. (2015). The Extracellular Domains of IgG1 and T Cell-Derived IL-4/IL-13 Are Critical for the Polyclonal Memory IgE Response In Vivo. *PLoS Biol.* 13, e1002290. <https://doi.org/10.1371/journal.pbio.1002290>.
11. He, J.S., Subramaniam, S., Narang, V., Srinivasan, K., Saunders, S.P., Carbojo, D., Wen-Shan, T., Hidayah Hamadee, N., Lum, J., Lee, A., et al. (2017). IgG1 memory B cells keep the memory of IgE responses. *Nat. Commun.* 8, 641. <https://doi.org/10.1038/s41467-017-00723-0>.
12. Ota, M., Hoehn, K.B., Fernandes-Braga, W., Ota, T., Aranda, C.J., Friedman, S., Miranda-Waldetario, M.G.C., Redes, J., Suprun, M., Grishina, G., et al. (2024). CD23+IgG1+ memory B cells are poised to switch to pathogenic IgE production in food allergy. *Sci. Transl. Med.* 16, eadi0673. <https://doi.org/10.1126/scitranslmed.adl0673>.
13. Koenig, J.F.E., Knudsen, N.P.H., Phelps, A., Bruton, K., Hoof, I., Lund, G., Libera, D.D., Lund, A., Christensen, L.H., Glass, D.R., et al. (2024). Type 2-polarized memory B cells hold allergen-specific IgE memory. *Sci. Transl. Med.* 16, eadi0944. <https://doi.org/10.1126/scitranslmed.adl0944>.
14. Tong, P., Granato, A., Zuo, T., Chaudhary, N., Zuiani, A., Han, S.S., Donthula, R., Shrestha, A., Sen, D., Magee, J.M., et al. (2017). IgH isotype-specific B cell receptor expression influences B cell fate. *Proc. Natl. Acad. Sci. USA.* 114, E8411–E8420. <https://doi.org/10.1073/pnas.1704962114>.
15. Achatz-Straussberger, G., Zaborsky, N., Königsberger, S., Luger, E.O., Lamers, M., Cramer, R., and Achatz, G. (2008). Migration of antibody secreting cells towards CXCL12 depends on the isotype that forms the BCR. *Eur. J. Immunol.* 38, 3167–3177. <https://doi.org/10.1002/eji.200838456>.
16. Aranda, C.J., Gonzalez-Kozlova, E., Saunders, S.P., Fernandes-Braga, W., Ota, M., Narayanan, S., He, J.S., Del Duca, E., Swaroop, B., Gnjatic, S., et al. (2023). IgG memory B cells expressing IL4R and FCER2 are associated with atopic diseases. *Allergy* 78, 752–766. <https://doi.org/10.1111/all.15601>.
17. Croote, D., Darmanis, S., Nadeau, K.C., and Quake, S.R. (2018). High-affinity allergen-specific human antibodies cloned from single IgE B cell transcriptomes. *Science* 362, 1306–1309. <https://doi.org/10.1126/science.aau2599>.
18. Ramonell, R.P., Brown, M., Woodruff, M.C., Levy, J.M., Wise, S.K., DelGaudio, J., Duan, M., Saney, C.L., Kyu, S., Cashman, K.S., et al. (2023). Single-cell analysis of human nasal mucosal IgE antibody secreting cells reveals a newly minted phenotype. *Mucosal Immunol.* 16, 287–301. <https://doi.org/10.1016/j.mucimm.2023.02.008>.
19. Calame, K.L., Lin, K.I., and Tunyaplin, C. (2003). Regulatory mechanisms that determine the development and function of plasma cells. *Annu. Rev. Immunol.* 21, 205–230. <https://doi.org/10.1146/annurev.immunol.21.120601.141138>.
20. Jiménez-Saiz, R., Chu, D.K., Mandur, T.S., Walker, T.D., Gordon, M.E., Chaudhary, R., Koenig, J., Saliba, S., Galipeau, H.J., Utley, A., et al. (2017). Lifelong memory responses perpetuate humoral TH2 immunity and anaphylaxis in food allergy. *J. Allergy Clin. Immunol.* 140, 1604–1615.e5. <https://doi.org/10.1016/j.jaci.2017.01.018>.
21. Lam, H.C.Y., and Jarvis, D.; ECRHS I Investigators (2021). Seasonal variation in total and pollen-specific immunoglobulin E levels in the European Community Respiratory Health Survey. *Clin. Exp. Allergy* 51, 1085–1088. <https://doi.org/10.1111/cea.13895>.
22. Bachert, C., Mannent, L., Naclerio, R.M., Mullol, J., Ferguson, B.J., Gevaert, P., Hellings, P., Jiao, L., Wang, L., Evans, R.R., et al. (2016). Effect of Subcutaneous Dupilumab on Nasal Polyp Burden in Patients With Chronic Sinusitis and Nasal Polyposis: A Randomized Clinical Trial. *JAMA* 315, 469–479. <https://doi.org/10.1001/jama.2015.19330>.
23. Beck, L.A., Thaçi, D., Hamilton, J.D., Graham, N.M., Bieber, T., Rocklin, R., Ming, J.E., Ren, H., Kao, R., Simpson, E., et al. (2014). Dupilumab treatment in adults with moderate-to-severe atopic dermatitis. *N. Engl. J. Med.* 371, 130–139. <https://doi.org/10.1056/NEJMoa1314768>.
24. Wenzel, S., Ford, L., Pearlman, D., Spector, S., Sher, L., Skobieranda, F., Wang, L., Kirkesseli, S., Rocklin, R., Bock, B., et al. (2013). Dupilumab in persistent asthma with elevated eosinophil levels. *N. Engl. J. Med.* 368, 2455–2466. <https://doi.org/10.1056/NEJMoa1304048>.
25. Bruton, K., Spill, P., Vohra, S., Baribeau, O., Manzoor, S., Gadkar, S., Davidson, M., Walker, T.D., Koenig, J.F.E., Ellenbogen, Y., et al. (2021). Interrupting reactivation of immunologic memory diverts the allergic response and prevents anaphylaxis. *J. Allergy Clin. Immunol.* 147, 1381–1392. <https://doi.org/10.1016/j.jaci.2020.11.042>.
26. Haniuda, K., Fukao, S., Kodama, T., Hasegawa, H., and Kitamura, D. (2016). Autonomous membrane IgE signaling prevents IgE-memory formation. *Nat. Immunol.* 17, 1109–1117. <https://doi.org/10.1038/ni.3508>.
27. Yang, Z., Robinson, M.J., Chen, X., Smith, G.A., Taunton, J., Liu, W., and Allen, C.D.C. (2016). Regulation of B cell fate by chronic activity of the IgE B cell receptor. *eLife* 5, e21238. <https://doi.org/10.7554/eLife.21238>.
28. Newman, R., and Tolar, P. (2021). Chronic calcium signaling in IgE+ B cells limits plasma cell differentiation and survival. *Immunity* 54, 2756–2771.e10. <https://doi.org/10.1016/j.immuni.2021.11.006>.
29. Laffleur, B., Duchez, S., Tarte, K., Denis-Lagache, N., Péron, S., Carrion, C., Denizot, Y., and Cogné, M. (2015). Self-Restrained B Cells Arise following Membrane IgE Expression. *Cell Rep.* 10, 900–909. <https://doi.org/10.1016/j.celrep.2015.01.023>.

30. Wade-Vallance, A.K., Yang, Z., Libang, J.B., Robinson, M.J., Tarlinton, D.M., and Allen, C.D.C. (2023). B cell receptor ligation induces IgE plasma cell elimination. *J. Exp. Med.* 220, e20220964. <https://doi.org/10.1084/jem.20220964>.
31. Savage, J., Sicherer, S., and Wood, R. (2016). The Natural History of Food Allergy. *J. Allergy Clin. Immunol. Pract.* 4, 196–203. <https://doi.org/10.1016/j.jaci.2015.11.024>.
32. Mitre, E., and Nutman, T.B. (2006). IgE memory: persistence of antigen-specific IgE responses years after treatment of human filarial infections. *J. Allergy Clin. Immunol.* 117, 939–945. <https://doi.org/10.1016/j.jaci.2005.12.1341>.
33. Holt, P.G., Sedgwick, J.D., O'Leary, C., Krska, K., and Leivers, S. (1984). Long-lived IgE- and IgG-secreting cells in rodents manifesting persistent antibody responses. *Cell. Immunol.* 89, 281–289. [https://doi.org/10.1016/0008-8749\(84\)90330-7](https://doi.org/10.1016/0008-8749(84)90330-7).
34. Luger, E.O., Fokuhl, V., Wegmann, M., Abram, M., Tillack, K., Achatz, G., Manz, R.A., Worm, M., Radbruch, A., and Renz, H. (2009). Induction of long-lived allergen-specific plasma cells by mucosal allergen challenge. *J. Allergy Clin. Immunol.* 124, 819–826.e4. <https://doi.org/10.1016/j.jaci.2009.06.047>.
35. Asrat, S., Kaur, N., Liu, X., Ben, L.H., Kajimura, D., Murphy, A.J., Sleeman, M.A., Limnander, A., and Orengo, J.M. (2020). Chronic allergen exposure drives accumulation of long-lived IgE plasma cells in the bone marrow, giving rise to serological memory. *Sci. Immunol.* 5, eaav8402. <https://doi.org/10.1126/sciimmunol.aav8402>.
36. Curotto de Lafaille, M.A., Muriglan, S., Sunshine, M.J., Lei, Y., Kutchukhidze, N., Furtado, G.C., Wensky, A.K., Olivares-Villagómez, D., and Lafaille, J.J. (2001). Hyper immunoglobulin E response in mice with monoclonal populations of B and T lymphocytes. *J. Exp. Med.* 194, 1349–1359. <https://doi.org/10.1084/jem.194.9.1349>.
37. Ting, J.P.-Y., and Trowsdale, J. (2002). Genetic Control of MHC Class II Expression. *Cell* 109, S21–S33. [https://doi.org/10.1016/S0092-8674\(02\)00696-7](https://doi.org/10.1016/S0092-8674(02)00696-7).
38. Koike, T., Fujii, K., Kometani, K., Butler, N.S., Funakoshi, K., Yari, S., Kikuta, J., Ishii, M., Kurosaki, T., and Ise, W. (2023). Progressive differentiation toward the long-lived plasma cell compartment in the bone marrow. *J. Exp. Med.* 220, e20221717. <https://doi.org/10.1084/jem.20221717>.
39. Wittner, J., Schulz, S.R., Steinmetz, T.D., Berges, J., Hauke, M., Channell, W.M., Cunningham, A.F., Hauser, A.E., Hutloff, A., Mielenz, D., et al. (2022). Krüppel-like factor 2 controls IgA plasma cell compartmentalization and IgA responses. *Mucosal Immunol.* 15, 668–682. <https://doi.org/10.1038/s41385-022-00503-0>.
40. Hu, S., Yang, K., Yang, J., Li, M., and Xiong, N. (2011). Critical roles of chemokine receptor CCR10 in regulating memory IgA responses in intestines. *Proc. Natl. Acad. Sci. USA.* 108, E1035–E1044. <https://doi.org/10.1073/pnas.1100156108>.
41. Watanabe, K., Sugai, M., Nambu, Y., Osato, M., Hayashi, T., Kawaguchi, M., Komori, T., Ito, Y., and Shimizu, A. (2010). Requirement for Runx proteins in IgA class switching acting downstream of TGF-beta 1 and retinoic acid signaling. *J. Immunol.* 184, 2785–2792. <https://doi.org/10.4049/jimmunol.0901823>.
42. Pak, H.K., Gil, M., Lee, Y., Lee, H., Lee, A.N., Roh, J., and Park, C.S. (2015). Regulator of G protein signaling 1 suppresses CXCL12-mediated migration and AKT activation in RPMI 8226 human plasmacytoma cells and plasmablasts. *PLoS One* 10, e0124793. <https://doi.org/10.1371/journal.pone.0124793>.
43. Shade, K.T., Conroy, M.E., and Anthony, R.M. (2019). IgE Glycosylation in Health and Disease. *Curr. Top. Microbiol. Immunol.* 423, 77–93. https://doi.org/10.1007/82_2019_151.
44. Jourdan, M., Cren, M., Robert, N., Bolloré, K., Fest, T., Duperray, C., Guilloton, F., Hose, D., Tarte, K., and Klein, B. (2014). IL-6 supports the generation of human long-lived plasma cells in combination with either APRIL or stromal cell-soluble factors. *Leukemia* 28, 1647–1656. <https://doi.org/10.1038/leu.2014.61>.
45. Zemskova, M., Sahakian, E., Bashkirova, S., and Lilly, M. (2008). The PIM1 kinase is a critical component of a survival pathway activated by docetaxel and promotes survival of docetaxel-treated prostate cancer cells. *J. Biol. Chem.* 283, 20635–20644. <https://doi.org/10.1074/jbc.M709479200>.
46. Weaver, K., and Skouta, R. (2022). The Selenoprotein Glutathione Peroxidase 4: From Molecular Mechanisms to Novel Therapeutic Opportunities. *Biomedicines* 10, 891. <https://doi.org/10.3390/biomedicines10040891>.
47. Feng, S., Wan, S., Liu, S., Wang, W., Tang, M., Bai, L., and Zhu, Y. (2022). LARS2 Regulates Apoptosis via ROS-Mediated Mitochondrial Dysfunction and Endoplasmic Reticulum Stress in Ovarian Granulosa Cells. *Oxid. Med. Cell. Longev.* 2022, 5501346. <https://doi.org/10.1155/2022/5501346>.
48. Carrington, E.M., Zhan, Y., Brady, J.L., Zhang, J.G., Sutherland, R.M., Anstee, N.S., Schenk, R.L., Vikstrom, I.B., Delconte, R.B., Segal, D., et al. (2017). Anti-apoptotic proteins BCL-2, MCL-1 and A1 summate collectively to maintain survival of immune cell populations both *in vitro* and *in vivo*. *Cell Death Differ.* 24, 878–888. <https://doi.org/10.1038/cdd.2017.30>.
49. Chevrier, S., Genton, C., Kallies, A., Karnowski, A., Otten, L.A., Malissen, B., Malissen, M., Botto, M., Corcoran, L.M., Nutt, S.L., et al. (2009). CD93 is required for maintenance of antibody secretion and persistence of plasma cells in the bone marrow niche. *Proc. Natl. Acad. Sci. USA.* 106, 3895–3900. <https://doi.org/10.1073/pnas.0809736106>.
50. Juliana, C.A., Yang, J., Rozo, A.V., Good, A., Groff, D.N., Wang, S.Z., Green, M.R., and Stoffers, D.A. (2017). ATF5 regulates β-cell survival during stress. *Proc. Natl. Acad. Sci. USA.* 114, 1341–1346. <https://doi.org/10.1073/pnas.1620705114>.
51. Ouchida, R., Kurosaki, T., and Wang, J.Y. (2010). A role for lysosomal-associated protein transmembrane 5 in the negative regulation of surface B cell receptor levels and B cell activation. *J. Immunol.* 185, 294–301. <https://doi.org/10.4049/jimmunol.1000371>.
52. Vecchione, A., Devlin, J.C., Tasker, C., Ramnarayan, V.R., Haase, P., Conde, E., Srivastava, D., Atwal, G.S., Bruhns, P., Murphy, A.J., et al. (2024). IgE plasma cells are transcriptionally and functionally distinct from other isotypes. *Sci. Immunol.* 9, eadm8964. <https://doi.org/10.1126/sciimmunol.adm8964>.
53. Pacheco, G.A., Rao, V., Yoo, D.K., Saghaei, S., Tong, P., Kumar, S., Marini-Rapoport, O., Allahyari, Z., Moghaddam, A.S., Esbati, R., et al. (2024). Origins and diversity of pan-isotype human bone marrow plasma cells. Preprint at bioRxiv. <https://doi.org/10.1101/2024.05.08.592267>.
54. Kabashima, K., Haynes, N.M., Xu, Y., Nutt, S.L., Allende, M.L., Proia, R.L., and Cyster, J.G. (2006). Plasma cell S1P1 expression determines secondary lymphoid organ retention versus bone marrow tropism. *J. Exp. Med.* 203, 2683–2690. <https://doi.org/10.1084/jem.20061289>.
55. Watanabe, H., Numata, K., Ito, T., Takagi, K., and Matsukawa, A. (2004). Innate immune response in Th1- and Th2-dominant mouse strains. *Shock* 22, 460–466. <https://doi.org/10.1097/01.shk.0000142249.08135.e9>.
56. Liu, X., Yao, J., Zhao, Y., Wang, J., and Qi, H. (2022). Heterogeneous plasma cells and long-lived subsets in response to immunization, autoantigen and microbiota. *Nat. Immunol.* 23, 1564–1576. <https://doi.org/10.1038/s41590-022-01345-s>.
57. Robinson, M.J., Ding, Z., Dowling, M.R., Hill, D.L., Webster, R.H., McKenzie, C., Pitt, C., O'Donnell, K., Mulder, J., Brodie, E., et al. (2023). Intrinsicly determined turnover underlies broad heterogeneity in plasma-cell lifespan. *Immunity* 56, 1596–1612.e4. <https://doi.org/10.1016/j.immuni.2023.04.015>.
58. Noval Rivas, M., Burton, O.T., Oettgen, H.C., and Chatila, T. (2016). IL-4 production by group 2 innate lymphoid cells promotes food allergy by blocking regulatory T-cell function. *J. Allergy Clin. Immunol.* 138, 801–811.e9. <https://doi.org/10.1016/j.jaci.2016.02.030>.
59. Kobayashi, T., Iijima, K., Dent, A.L., and Kita, H. (2017). Follicular helper T cells mediate IgE antibody response to airborne allergens. *J. Allergy Clin. Immunol.* 139, 300–313.e7. <https://doi.org/10.1016/j.jaci.2016.04.021>.

60. O'Connor, B.P., Raman, V.S., Erickson, L.D., Cook, W.J., Weaver, L.K., Ahonen, C., Lin, L.L., Mantchev, G.T., Bram, R.J., and Noelle, R.J. (2004). BCMA is essential for the survival of long-lived bone marrow plasma cells. *J. Exp. Med.* 199, 91–98. <https://doi.org/10.1084/jem.20031330>.
61. Rebello, R.J., Huglo, A.V., and Furic, L. (2018). PIM activity in tumours: A key node of therapy resistance. *Adv. Biol. Regul.* 67, 163–169. <https://doi.org/10.1016/j.jbior.2017.10.010>.
62. Avery, D.T., Kalled, S.L., Ellyard, J.I., Ambrose, C., Bixler, S.A., Thien, M., Brink, R., Mackay, F., Hodgkin, P.D., and Tangye, S.G. (2003). BAFF selectively enhances the survival of plasmablasts generated from human memory B cells. *J. Clin. Invest.* 112, 286–297. <https://doi.org/10.1172/JCI18025>.
63. Benson, M.J., Dillon, S.R., Castiglione, E., Geha, R.S., Xu, S., Lam, K.-P., and Noelle, R.J. (2008). Cutting Edge: The Dependence of Plasma Cells and Independence of Memory B Cells on BAFF and APRIL1. *J. Immunol.* 180, 3655–3659. <https://doi.org/10.4049/jimmunol.180.6.3655>.
64. Mohr, E., Serre, K., Manz, R.A., Cunningham, A.F., Khan, M., Hardie, D.L., Bird, R., and MacLennan, I.C.M. (2009). Dendritic cells and monocyte/macrophages that create the IL-6/APRIL-rich lymph node microenvironments where plasmablasts mature. *J. Immunol.* 182, 2113–2123. <https://doi.org/10.4049/jimmunol.0802771>.
65. Shade, K.C., Conroy, M.E., Washburn, N., Kitaoka, M., Huynh, D.J., Laprise, E., Patil, S.U., Shreffler, W.G., and Anthony, R.M. (2020). Sialylation of immunoglobulin E is a determinant of allergic pathogenicity. *Nature* 582, 265–270. <https://doi.org/10.1038/s41586-020-2311-z>.
66. Shade, K.T.C., Platzer, B., Washburn, N., Mani, V., Bartsch, Y.C., Conroy, M., Pagan, J.D., Bosques, C., Mempel, T.R., Fiebiger, E., and Anthony, R. M. (2015). A single glycan on IgE is indispensable for initiation of anaphylaxis. *J. Exp. Med.* 212, 457–467. <https://doi.org/10.1084/jem.20142182>.
67. Cheng, Q., Khodadadi, L., Taddeo, A., Klotsche, J., F Hoyer, B., Radbruch, A., and Hiepe, F. (2018). CXCR4-CXCL12 interaction is important for plasma cell homing and survival in NZB/W mice. *Eur. J. Immunol.* 48, 1020–1029. <https://doi.org/10.1002/eji.201747023>.
68. Milcarek, C., and Hall, B. (1985). Cell-specific expression of secreted versus membrane forms of immunoglobulin gamma 2b mRNA involves selective use of alternate polyadenylation sites. *Mol. Cell. Biol.* 5, 2514–2520. <https://doi.org/10.1128/mcb.5.10.2514-2520.1985>.
69. Robinson, M.J., Dowling, M.R., Pitt, C., O'Donnell, K., Webster, R.H., Hill, D.L., Ding, Z., Dvorscek, A.R., Brodie, E.J., Hodgkin, P.D., et al. (2022). Long-lived plasma cells accumulate in the bone marrow at a constant rate from early in an immune response. *Sci. Immunol.* 7, eabm8389. <https://doi.org/10.1126/sciimmunol.abm8389>.
70. Manakkat Vijay, G.K., Zhou, M., Thakkar, K., Rothrauff, A., Chawla, A.S., Chen, D., Lau, L.C.W., Gerges, P.H., Chetal, K., Chhibbar, P., et al. (2024). Temporal dynamics and genomic programming of plasma cell fates. *Nat. Immunol.* 25, 1097–1109. <https://doi.org/10.1038/s41590-024-01831-y>.
71. Jing, Z., Galbo, P., Ovando, L., Demouth, M., Welte, S., Park, R., Chandran, K., Wu, Y., MacCarthy, T., Zheng, D., et al. (2024). Fine-tuning spatial-temporal dynamics and surface receptor expression support plasma cell-intrinsic longevity. *eLife* 12, RP89712. <https://doi.org/10.7554/eLife.89712>.
72. Flamar, A.L., Klose, C.S.N., Moeller, J.B., Mahlakõiv, T., Bessman, N.J., Zhang, W., Moriyama, S., Stokic-Trtica, V., Rankin, L.C., Putzel, G.G., et al. (2020). Interleukin-33 Induces the Enzyme Tryptophan Hydroxylase 1 to Promote Inflammatory Group 2 Innate Lymphoid Cell-Mediated Immunity. *Immunity* 52, 606–619.e6. <https://doi.org/10.1016/j.jimmuni.2020.02.009>.
73. Amend, S.R., Valkenburg, K.C., and Pienta, K.J. (2016). Murine Hind Limb Long Bone Dissection and Bone Marrow Isolation. *J. Vis. Exp.* 53936. <https://doi.org/10.3791/53936>.
74. Stuart, T., Butler, A., Hoffman, P., Hafemeister, C., Papalexi, E., Mauck, W. M., III, Hao, Y., Stoeckius, M., Smibert, P., and Satija, R. (2019). Comprehensive Integration of Single-Cell Data. *Cell* 177, 1888–1902.e21. <https://doi.org/10.1016/j.cell.2019.05.031>.
75. Giudicelli, V., Chaume, D., and Lefranc, M.P. (2005). IMGT/GENE-DB: a comprehensive database for human and mouse immunoglobulin and T cell receptor genes. *Nucleic Acids Res.* 33, D256–D261. <https://doi.org/10.1093/nar/gki010>.
76. Ye, J., Ma, N., Madden, T.L., and Ostell, J.M. (2013). IgBLAST: an immunoglobulin variable domain sequence analysis tool. *Nucleic Acids Res.* 41, W34–W40. <https://doi.org/10.1093/nar/gkt382>.
77. Gupta, N.T., Vander Heiden, J.A., Uduman, M., Gadala-Maria, D., Yaari, G., and Kleinstein, S.H. (2015). Change-O: a toolkit for analyzing large-scale B cell immunoglobulin repertoire sequencing data. *Bioinformatics* 31, 3356–3358. <https://doi.org/10.1093/bioinformatics/btv359>.

STAR★METHODS

KEY RESOURCES TABLE

REAGENT or RESOURCE	SOURCE	IDENTIFIER
Antibodies		
Brilliant Violet 421 anti-mouse CD138 (Syndecan-1)	BioLegend	Cat# 142508; RRID: AB_11203544
Pacific Blue anti-mouse Ly-6A/E (Sca-1) (D-7)	BioLegend	Cat# 108120; RRID: AB_493273
Brilliant Violet 510 anti-mouse CD326 (Ep-CAM)	BioLegend	Cat# 118231; RRID: AB_2632774
BV650 Rat Anti-Mouse IgA	BD Biosciences	Cat# 743296; RRID: AB_2741407
Super Bright 702 Rat anti-mouse CD93	Thermo Fisher Scientific	Cat# 67-5892-82; RRID: AB_2762798
BV750 Rat Anti-Mouse CD23	BD Biosciences	Cat# 746946; RRID: AB_2871733
FITC Rat Anti-Mouse I-A/I-E (2G9)	BD Biosciences	Cat# 553623; RRID: AB_394958
Alexa Fluor 532, anti Ki-67	Thermo Fisher Scientific	Cat# 58-5698-82; RRID: AB_2802365
PerCP anti-mouse CD3ε	BioLegend	Cat# 100325; RRID: AB_893319
Spark UV 387 anti-mouse Ly-6C	BioLegend	Cat# 128059; RRID: AB_3083272
PE/Dazzle 594 anti-human/mouse Integrin β7	BioLegend	Cat# 321225; RRID: AB_2715982
PE-Cyanine5 anti-mouse IgM	Thermo Fisher Scientific	Cat# 15-5790-82; RRID: AB_494222
PE/Cyanine7 anti-mouse IgG1 (RMG1-1)	BioLegend	Cat# 406614; RRID: AB_2562002
FITC anti-BrdU	BioLegend	Cat# 364104; RRID: AB_2564481
APC/Fire 750 anti-mouse CD98 (4F2)	BioLegend	Cat# 128216; RRID: AB_2750549
APC/Fire 810 anti-mouse/human CD45R/B220	BioLegend	Cat# 103277; RRID: AB_2860603
Brilliant Violet 785 anti-mouse I-A/I-E (M5/114.15.2)	BioLegend	Cat# 107645; RRID: AB_2565977
Alexa Fluor 700 anti-mouse F4/80	Biolegend	Cat# 123129; RRID: AB_2277848
PE anti-mouse CD23 (B3B4)	BioLegend	Cat# 101607; RRID: AB_312832
PE/Cyanine7 anti-mouse IgG1 (M1-14D12)	Thermo Fisher Scientific	Cat# 25-4015-82; RRID: AB_11150243
PerCP/Cy5.5 anti-mouse Ly-6C (HK1.4)	Biolegend	Cat# 128011; RRID: AB_1659242
BV605 Rat Anti-Mouse CD319(SLAMF7)	BD Biosciences	Cat# 747996; RRID: AB_2872457
Alexa Fluor 700 anti-mouse CD3 (17A2)	BioLegend	Cat# 100216; RRID: AB_493697
Alexa Fluor 647 Anti-Mouse IgE (R1E4)	in house	N/A
Alexa Fluor 488 Anti-Mouse IgE (R1E4)	in house	N/A
Unlabeled Anti-Mouse IgE (R1E4)	in house	N/A
Goat F(ab')2 Anti-Mouse IgG1	SouthernBiotech	Cat# 1072-01; RRID: AB_2794431
Purified Rat Anti-Mouse IgE (R35-72)	BD Biosciences	Cat# 553413; RRID: AB_394846
Purified Mouse IgE κ Isotype Control (C38-2)	BD Biosciences	Cat# 557079; RRID: AB_479637
Purified Mouse Anti-Human Light Chain, λ	BD Biosciences	Cat# 555793; RRID: AB_396128
Rat Anti-Mouse IgE-HRP	SouthernBiotech	Cat# 1130-05; RRID: AB_2794618
Goat F(ab')2 Anti-Mouse IgG1	SouthernBiotech	Cat# 1072-08; RRID: AB_2794433
CD16/CD32 Monoclonal Antibody	Thermo Fisher Scientific	Cat# 14-0161-82; RRID: AB_467133
FITC anti-mouse IgM (RMM-1)	BioLegend	Cat# 406506; RRID: AB_315056
Rat IgG2a isotype control	Bio X Cell	Cat#BE0089; RRID: AB_1107769
Rat Anti-Mouse Kappa-UNLB	SouthernBiotech	Cat#1170-01; RRID: AB_2794662
BV650 Rabbit Anti- Active Caspase-3	BD Biosciences	Cat#564096; RRID: AB_2738589
eFluor 660 Anti-mouse CD79a	Thermo Fisher Scientific	Cat#50079180; RRID: AB_11217884
Chemicals, peptides, and recombinant proteins		
Tamoxifen	ThermoFisherScientific	Cat# J63509.03
Imject alum	ThermoFisherScientific	Cat.#77161
Sunflower seed oil	Sigma	Cat# S5007
ACK lysing buffer	GIBCO	Cat# A10492-01

(Continued on next page)

Continued

REAGENT or RESOURCE	SOURCE	IDENTIFIER
DNAse I	Sigma	Cat# D4513
Zombie Acqua (L/D Blue)	BioLegend	Cat# 423102
TMB substrate set	BioLegend	Cat# 421101
Sulfuric acid (0.5M)	LabChem	Cat# LC257704
Protein G Sepharose 4 Fast Flow	Sigma-Aldrich	Cat# GE17-0618-01
DPBS	Gibco	Cat# 14190250
0.5M EDTA, pH8.0	Invitrogen	Cat# 15575038
Tween 20	Sigma-Aldrich	Cat# 9005-64-5
BSA	Biosearch Technologies	Cat# N-5050H-10
CD138 MicroBeads, mouse	Miltenyi Biotec	Cat# 130-098-257
BrdU (5-Bromo-2'-Deoxyuridine)	Invitrogen	Cat# B23151
Cyto-Fast Perm Wash Buffer set	BioLegend	Cat# 426803
Formamide	ThermoFisherScientific	BP227-100
RNeasy plus mini kit	Qiagen	Cat# 74134
Ovation Trio low input RNA Library Systems V2	Nugen	Cat# 0507-08
RPMI 1640 Medium, GlutaMAX	ThermoFisherScientific	Cat# 61870036
HEPES 1M Solution	Global Life Sciences Solutions	Cat# SH30237.01
MEM Non-Essential Amino Acids (100X)	Gibco	Cat# 11140-050
Streptavidin HRP	BD Biosciences	Cat# 554066
<i>Alternaria alternata</i> extract	Greer Laboratories	Cat# 362083
Albumin from chicken egg	Sigma	A5253-250G
HA (YPYDVPDYASLRS)	Thermo Fisher Scientific	N/A
PEP1 (YPYDVPDFASLRS)	Thermo Fisher Scientific	N/A
Streptavidin HRP	BD Biosciences	Cat# 550946
Zombie Aqua Fixable Viability Kit	BioLegend	Cat# 423102
Mouse IL-6 Recombinant Protein	PeproTech	Cat# 216-16
Highly purified SEB	Toxin Technologies	Cat# NC9442400
Mouse APRIL Recombinant Protein	PeproTech	Cat# 315-13
Deposited data		
Mouse bulk RNA-seq	this paper	BioProject: PRJNA1289849
Mouse scRNA-seq	this paper	BioProject: PRJNA1200005
Experimental models: Organisms/strains		
T-B monoclonal mice (TBmc)	Curotto de Lafaille et al. ³⁶	N/A
B6.Cg-Gt(ROSA)26Sortm14 (CAG-tdTomato)Hze/J	Jackson Laboratory	Strain #007914; RRID: IMSR_JAX:007914
C.129S7(B6)-Rag1tm1Mom/J	Jackson Laboratory	Strain #003145; RRID: IMSR_JAX:007914
<i>PRDM1CreERT2</i>	This paper	N/A
<i>Nippostrongylus brasiliensis</i>	Flamar et al. ⁷²	N/A
<i>IL4ra Y709F</i>	N/A	RRID: IMSR_JAX:012709
Oligonucleotides		
<i>PRDM1CreERT2</i> Genotyping (FW) CTTCTGGTCTCCCGAGGTTT	This paper	N/A
<i>PRDM1CreERT2</i> Genotyping (RW) CATCGACCGGTAAATGCAGGC	This paper	N/A
Software and algorithms		
Cytobank	Beckman Coulter	https://www.cytobank.org
FlowJo v10	Becton, Dickinson Company	https://www.flowjo.com
GraphPad Prism v8.3.0	GraphPad Software	https://www.graphpad.com

(Continued on next page)

Continued

REAGENT or RESOURCE	SOURCE	IDENTIFIER
IDEAS	Luminex Corp.	https://www.luminexcorp.com/download/amnis-ideas-software-user-manual/
Imaris 9.5.1	Bitplane, Oxford Instruments	N/A
INSPIRE	Luminex Corp.	https://www.luminexcorp.com/flowsight-imaging/#software
Adobe Illustrator	Adobe	https://www.adobe.com/products/illustrator.html ; RRID: SCR_014198
Seurat R Package v5.1.0	Satija et al.	https://github.com/satijalab/seurat
R	The R Project for Statistical Computing	https://www.r-project.org .
Cell Ranger	10x Genomics	https://www.10xgenomics.com/support/software/cell-ranger/latest
Enrichr	Ma'ayan Lab	https://maayanlab.cloud/Enrichr/
scDissector	GitHub	https://www.10xgenomics.com/support/software/cell-ranger/latest
ComplexHeatmap	Bioconductor	https://jokergoo.github.io/ComplexHeatmap-reference/book/
ggplot2	CRAN	https://ggplot2.tidyverse.org/
tidyverse	CRAN	https://www.tidyverse.org/
matrix	CRAN	https://cran.r-project.org/web/packages/Matrix/index.html
seriation	CRAN	https://cran.r-project.org/web/packages/seriation/
dream	GitHub / Bioconductor	https://github.com/GabrielHoffman/Dream
SingleR	Bioconductor	https://bioconductor.org/packages/release/bioc/html/SingleR.html
CellChat	GitHub	https://bioconductor.org/packages/release/bioc/html/SingleR.html
Dirichlet	CRAN	https://cran.r-project.org/web/packages/DirichletReg/index.html
Immunarch	GitHub	https://cran.r-project.org/web/packages/survminer/index.html
Survminer	CRAN	https://cran.r-project.org/web/packages/survminer/index.html
gtsummary	CRAN	https://cran.r-project.org/web/packages/gtsummary/index.html
TRUST4	Liu Lab	https://github.com/liulab-dfci/TRUST4
MiXCR	GitHub	https://github.com/milaboratory/mixcr
Monocle3	Trapnell Lab	https://cole-trapnell-lab.github.io/monocle-release/

EXPERIMENTAL MODEL AND STUDY PARTICIPANT DETAILS**Mouse strains**

TBmc mice. TBmc mice express TCR $\alpha\beta$ chains specific for the MHCII-restricted peptide 323-339 from chicken ovalbumin (OVA); and knock-in immunoglobulin heavy and light chain V(D)J genes encoding an antibody against a linear peptide (YPYDVPDYASLRS) from the influenza hemagglutinin protein. These mice are on a BALB/c RAG1 $^{-/-}$ background. TBmc mice heterozygous for the V(D)J gene knock-ins and TCR transgenes were used in the experiments.

Prdm1^{CreERT2} R26^{tdT} mice. Mice expressing a tamoxifen-inducible cre gene (*creERT2*) under the control of the *Prdm1* regulatory sequences (*Prdm1*^{CreERT2} mice) were generated using CRISP/Cas9 methodology. The stop codon of the *Prdm1* gene in exon 7 was replaced with a 2A ribosomal skipping sequence linked to the *creERT2* coding sequence (Figure S6). For the targeting vector, the 2A-*creERT2* sequence was linked to a homology sequence 573 nucleotides long at 5' and a 1168 nucleotide long homology sequence at 3'. Oocytes were injected with annealed crRNA and tracerRNA (from IDT) together with Cas9 protein (Sigma eSpCas9 Protein #cas9prot) and 2 guide RNAs flanking the insertion site. A mouse with the correct insertion was identified using PCR on genomic DNA.

Prdm1^{CreERT2} mice were crossed with *Rosa26-stop-tdTomato* (*R26*^{tdT}) mice (The Jackson Laboratories #007914) to generate *Prdm1*^{CreERT2}*R26*^{tdT} mice.

Mice were maintained under specific-pathogen-free conditions in the animal facility of Mount Sinai. All animal experiments performed in this study were approved by the Institutional Animal Care and Use Committee of the Icahn School of Medicine at Mount Sinai (IUC protocol 2019-0040).

Immunizations and infections

Mice were immunized by intraperitoneal injection with 100 µg of OVA crosslinked to the hemagglutinin mutant peptide PEP1 (OVA-PEP1) or NP-OVA (Biosearch Technologies N50511000) or NP-KLH (Biosearch Technologies NC0574994) in 1mg of alum. Multiple immunizations were performed with a 21 to 30 days interval between each injection. PEP1 (YPYDVPPDFASLRS) carries phenylalanine in place of tyrosine 105, a mutation that greatly diminishes BCR affinity in TBmc mice.⁵ *Prdm1*^{CreERT2}*R26*^{tdT} mice were infected with 400-500 L3 larvae from the helminth parasite *Nippostrongylus brasiliensis* via subcutaneous dorsal injection. Secondary infections were performed 30 days afterwards.

To model chronic asthma, *Alternaria alternata* extract (Lots 364361 and 362083; Greer, Lenoir, NC, USA) was administered intra-nasally to *Prdm1*^{CreERT2}*R26*^{tdT} mice for 10 weeks. In the first 2 weeks (weeks -10 and -9), mice received 25 ng of *A. alternata* once a week; in the following 6 weeks (week -8 to -3), they received 10 ng once a week. In the last 2 weeks (weeks -2 and -1), they received three 10 ng doses per week.

For the peanut allergy model, IL4raF709 mice received by oral gavage 22.5 mg of peanut butter dissolved in 1.3% sodium bicarbonate (200µl per mouse) once a week for 6 weeks. 10 µg of staphylococcal enterotoxin B (SEB; Toxin Technolog FL NC9442400) was added to the first 2 intragastric sensitizations. Mice were infected or immunized at 8 to 10 weeks of age. Both males and females were used for experiments, with no significant differences noted between sexes.

BrdU incorporation

Mice were fed BrdU 0.5 mg/ml + 1% sucrose solution through their drinking water for 14 days before euthanasia.

Tamoxifen treatment

Tamoxifen (Thermo Scientific, #J63509.03) was diluted in sunflower seed oil (Sigma #S5007) to a concentration of 50 mg/ml and incubated at 37°C overnight. 100 ml of the tamoxifen solution was then administered to mice by oral gavage at the time and frequencies indicated in the figures' legends.

METHOD DETAILS

ELISA

Plasma samples were separated by centrifugation from heparinized blood and were kept frozen until analysis. To measure total IgE or total IgG1, Immulon 4 HBX 96 well plates (Thermo scientific # 3855) were coated with 2mg/ml of purified rat anti-mouse IgE antibodies in PBS (clone R35-72, BD Biosciences) or Goat F(ab')2 Anti-Mouse IgG1 in PBS, respectively. For the quantification of PEP1-specific antibodies, plates were coated with 10mg of PEP1 in PBS. Plates were incubated overnight at 4°C, washed with washing buffer (0.05% Tween-20 in PBS) and then blocked with a solution of 1% bovine serum albumin (BSA) in washing buffer for one hour at room temperature (RT). After washing, serially diluted plasma samples and purified immunoglobulin standards were added to the plates and incubated overnight at 4°C. To quantify PEP1-specific IgE, samples were incubated beforehand with Protein G Sepharose (Sigma-Aldrich # GE17-0618-01) to deplete IgG antibodies. After sample incubation, the plates were washed, and secondary antibodies were added. To detect IgE antibodies, horseradish peroxidase (HRP)-labeled anti-IgE antibodies diluted 1:2000 (SouthernBiotech #1130-05;) were added to the wells, and plates were incubated for 2 hours at RT. To detect IgG1 antibodies, biotinylated anti-mouse IgG1 (Southern Biotech #1072-08) was added to the wells at a concentration of 0.25mg. The plates were incubated for 2 hours at RT, then washed and incubated with streptavidin-HRP (BD Biosciences #554066) at 1:5000 dilution for 30 minutes at RT. Plates were then washed and subsequently developed with TMB Substrate solution (BioLegend, #421101). The reactions were stopped by adding 2M H₂SO₄ and subsequently read at OD450 on a microplate reader Molecular Devices SpectraMax. Titers were defined as the plasma dilution at which the OD450 signal reached 50% of the maximum OD obtained on the plate.

Preparation of OVA-PEP1 crosslinked antigen

The OVA-PEP1 antigen was generated by glutaraldehyde-mediated crosslinking of the PEP1 peptide to chicken ovalbumin (OVA). Briefly, OVA was dissolved at 20 mg/ml in 0.1 M borate buffer, pH 10. The PEP1 peptide was dissolved separately at 100 mg/ml in sterile water and added to the OVA solution to reach a final OVA concentration of 10 mg/ml. After mixing, an equal volume of freshly prepared 0.3% glutaraldehyde in borate buffer pH 10 was added dropwise under constant agitation. The reaction proceeded for 2 hours at RT on a nutator and was then quenched by the addition of 83 µl of 1 M glycine per ml of reaction volume. The mixture was rotated for an additional 30 minutes and transferred into dialysis tubing. Dialysis was performed overnight at 4°C against 0.1 M borate buffer pH 8.5 (2x), sterile water (1x), and PBS (1x). The final volume was measured, aliquoted, and stored at -80°C.

IgG antibody depletion from plasma

Protein G Sepharose beads (Sigma-Aldrich, #GE17-0618-01) were washed three times with PBS containing 10 mM EDTA by centrifugation at 2000 rpm for 1 minute. Subsequently, 50 µL of beads were added to 200 µL of mouse plasma. The mixture was incubated overnight at 4 °C on a rotating nutator. The IgG-depleted plasma was collected after centrifugation.

Flow cytometry

Spleen and mesenteric lymph nodes were collected in staining buffer (PBS with 2% FBS, 4mM EDTA and 0.02% sodium azide) and mashed through a 70-µm cell strainer to prepare a single cell suspension. Bone marrow isolation was performed as described.⁷³ Red blood cells were lysed using ACK Lysing Buffer (Gibco #A1049201). Prior to surface staining, cells were incubated with fixable viability dye (BioLegend #423102) diluted 1:5000 in PBS for 10 minutes at RT, followed by Fc block (Invitrogen, #14-0161-86, anti CD16/CD32 Clone 93) diluted 1:100 for 5 minutes at RT. Cell surface staining was performed for 15 minutes at RT. Immunoglobulins, Ki-67 and BrdU were stained intracellularly.

For intracellular staining, cells were fixed and permeabilized with Cyto-Fast Fix/Perm Buffer (BioLegend #426803) according to the manufacturer's instructions. Cells were then incubated with antibodies overnight at 4°C and then washed 4 times. For BrdU staining, a second round of permeabilization was performed using 1% PFA and 0.5% Tween 20 in PBS for 30 minutes at RT. The cells were then washed with PBS containing Ca²⁺ and Mg²⁺, and incubated with 300mg/ml of DNaseI (Sigma #D4513) in the same buffer for 15 min 37°C. The cells were then incubated with anti-BrdU antibody added to the intracellular antibody mix for 45 minutes at 4°C. After staining, the cells were resuspended in staining buffer for analysis in a flow cytometer or for cell sorting. Cells were analyzed in a CytoFLEX Cytometer (Beckman Coulter) using CytExpert Software, or in a Cytek Aurora Spectral Cytometer (Cytek) using SpectroFlo Software v.3.0. For cell sorting, cells were acquired in a FACSAria cell sorter (BD) using FACSDiva software version 6.0. Flow cytometry analysis was performed using Cytobank and FlowJo softwares. The antibodies used for flow cytometry are described in the Key resources file.

Quantification of surface and intracellular IgE

Splenic plasma cells were isolated from TBmc mice 30 or 150 days after immunization. The cells from both time points were pooled, and PCs were purified using anti-mouse CD138 MicroBeads (Miltenyi Biotec #130-098-257). Subsequently, the cells were surface stained with BV421-labeled anti-CD138 (clone 281-2), BV785 labeled anti-MHCII (clone B3B4), and Alexa 647-labeled anti-IgE (clone RIE4). After washing, cells were permeabilized and stained intracellularly with Alexa 488-labeled anti-IgE (clone RIE4). The expression of surface IgE (IgE SF), intracellular IgE (IgE IC), MHCII, CD138 was evaluated in single cells using flow cytometry images acquired with the AMNIS imaging flow cytometer (Cytek) and analyzed using IMARIS software. IgE PCs were identified by CD138 and IgE IC expression.

BCR crosslinking assay on mature IgE plasma cells

For ex-vivo experiments, spleens from TBmc mice were collected from mice 16- and 150- days post-immunization. Single-cell suspensions were prepared and plated at 10⁷ cells per well in complete culture medium. Cells were incubated with isotype control (2A3), anti-IgE (R1E4), or anti-kappa light chain (187.1) antibodies to induce BCR crosslinking at a final concentration of 2.5 µg/ml. After 6 or 24 hours of incubation at 37°C, IgE PCs numbers were quantified by flow cytometry. Data were expressed as absolute cell counts per well or as percentages of remaining IgE PCs normalized to the corresponding isotype control.

To evaluate spontaneous apoptosis, untreated cells were intracellularly stained for active caspase-3 (C92-605) after a 6 hours incubation.

For In-vivo test *Prdm1*^{CreERT2} × *Rosa26*^{tdT} mice were immunized intraperitoneally with NP-OVA in alum. At day 35 post-immunization, PCs were time-stamped by administering tamoxifen via oral gavage on two consecutive days (days 35 and 36). Three days after the final tamoxifen dose (day 39), mice received a secondary immunization with NP-OVA in alum. 7 days later (day 46) mice were injected intravenously with 3.25 mg/kg of either anti-IgE monoclonal antibody (clone R1E4) or an isotype control antibody (2A3). Mice were euthanized 24 hours later for analysis. Spleens were harvested and processed for flow cytometry to quantify total and tdTomato+ (time-stamped) IgE PCs.

Passive cutaneous anaphylaxis assay

For the passive cutaneous anaphylaxis assay (PCA), 10 µl of IgG-depleted plasma were injected intradermally into the ears of 8- to 10-week-old naive BALB/c mice. Twenty-four hours later, the mice were injected intravenously with 50 µg of *Alternaria alternata* extract in 1% Evans Blue PBS. The mice were euthanized 30 minutes later. The extravasation of Evans Blue, indicating increased vascular permeability due to anaphylaxis, was quantified by soaking the ear tissue overnight in 700 µL of formamide (BP227-100) at 65°C and reading the resulting solutions at OD620 on a microplate reader Molecular Devices SpectraMax.

Antibody secretion assay

PCs were isolated from the pooled spleens of 10 TBmc mice 8 days after a third immunization using anti-mouse CD138 MicroBeads (Miltenyi Biotec #130-098-257). To assess antibody production and cell survival, PCs were cultured in RPMI-1640 medium (Thermo Fisher 61870036) with 10% FBS (Thermo Scientific 10439024), 20ng/ml of IL6 (PeproTech 216-16) and 200ng/ml of APRIL (PeproTech 315-13) for 24 hours. Cells and supernatants were collected at hours 3, 18, and 24 for flow cytometry analysis and for

antibody quantification by ELISA. Antibody secretion per cell was calculated by multiplying antibody concentration ($\mu\text{g}/\text{ml}$) by culture volume (0.2 ml) and dividing by the number of PCs per well.

Bulk RNAseq

RNA was isolated from the sorted PCs of BALB/c mice 8 days after *Nippostrongylus brasiliensis* infection using Qiagen RNeasy plus mini kit (74134). RNA quality was assessed using Pico Bioanalyser chips (Agilent; 5067-1513). Only RNAs displaying an RNA integrity number of 9 or higher were used for downstream procedures. RNAseq libraries were prepared using the Nugen Ovation Trio low input RNA Library Systems V2 (Nugen; 0507-08) according to the manufacturer's instructions by the NYU Genome Technology Center. Libraries were sequenced as 50-nucleotide, paired-end reads on an Illumina HiSeq 2500 using v4 chemistry. RNAseq data quality assessment and visualization Illumina sequencing adapters and reads with Phred quality scores <20 were removed with Trimmomatic. Trimmed reads were mapped to the *Mus musculus* genome using STAR v2.5.3a with default settings. The number of reads uniquely mapping to each gene feature in the corresponding annotation file was determined using feature Counts. The resulting count tables were passed to R for further analyses.

10X Genomics scRNAseq

Spleen, mesenteric lymph nodes, and bone marrow were collected from 10 TBmc mice. Prior to the experiment, the mice were immunized three times with OVA-PEP1+alum, with 21-30-day intervals between each injection. Cells were harvested 21 days after the last immunization. After generating single cell suspensions from the tissues, PCs were purified using anti-mouse CD138 MicroBeads (Miltenyi Biotec, #130-098-257) according to the manufacturer's instructions. Hash-tagged antibodies were then added to each sample and the cells were incubated with fluorescently labeled antibodies to CD98 (clone RL388), CD138 (clone 281-2), IgG1(clone M1-14D12), IgE (clone R1E4), and IgM (clone RMM-1) for 15 minutes at RT. $\text{CD98}^+\text{CD138}^+\text{IgM}^-$ PC populations were sorted on a FACSaria II (BD Biosciences). After confirming cell count and viability, PCs from the spleen, lymph nodes, and bone marrow were combined in equal proportions and loaded on a Chromium 10X controller using 5' chemistry (10X Genomics) with an expected recovery of 10,000 cells per lane according to the manufacturer's protocol. Libraries were prepared and sequenced on a HiSeq2500.

Single cell gene expression analysis

Gene expression reads were aligned to the mouse mm10 genome of reference transcriptome and count matrices were generated using the default CellRanger 2.1 workflow, using the 'raw' matrix output. Following alignment, only cell barcodes with >200 unique genes and ≤ 1000 total counts were included in the analysis. From this subset, cells in which mitochondrial transcripts made up more than 25% of total expression were excluded from downstream analyses. Cell quality control thresholds were applied to ensure robust downstream analysis. Matrix scaling, logarithmic normalization, and batch correction via data alignment through canonical correlation analysis, and unsupervised clustering using a K-nn graph partitioning approach were performed as previously described.⁷⁴ To avoid isotype-driven segregation, data was clustered to exclude immunoglobulin heavy chain genes associated with each isotype. Differentially expressed genes were identified using the FindMarkers function (Seurat). To further analyze the markers of interest, imputed mean UMI counts were used to calculate log-fold changes in gene expression between different cell states. Other R packages used include: scDissector v.1.0.0; ComplexHeatmap v.2.0; ggplot2 v.3.3.5; tidyverse v.1.0; Matrix v.0.9.8; seriation v.1.3.5. Dream v.1.0, singleR v.1.0, cellchat v.1.0, DirichLet v.0.9, and Immunarch v.1.5. Differential abundance was assessed using Dirichlet regression modeling strategies. BCR analysis was done using immunarch and the Wilcoxon rank test. Reconstruction of BCRs from bulk and single cell data was done using TRUST4 and MixCR algorithms. Trajectory analyses were conducted using Monocle V3 and Moran's I index.

Functional scoring and pathway analysis

Cells were scored using gene sets from Gene Ontology functional pathways, including modules related to response to ER stress (GO:0034976), translation (GO:0006417), and N-glycosylation processes (GO:0006487). Scores were calculated using Seurat's AddModuleScore function.

Analysis comparison across species

We filtered for differentially expressed genes (DEGs) with P values < 0.05 from both spleen and bone marrow mature IgE⁺ PCs. These mouse genes were then converted to their human orthologs using the HomoloGene package. Genes that could not be mapped were excluded, resulting in a final set of 750 converted genes.

Raw gene expression data from the Pacheco et al.⁵³ and Vecchione et al.⁵² Datasets were retrieved from the NCBI database and processed into Seurat objects. Following standard preprocessing, proliferating cells were excluded based on MKI67 expression. DEGs for bone marrow IgE⁺ PCs were identified using the FindMarkers function in Seurat.

We focused our downstream analysis on only the genes present in all 3 datasets. To identify commonly enriched genes, we filtered based on average log fold change (avg_log2FC > 0) and then intersected our converted DEG list with the DEGs from the remaining genes described by Pacheco et al.⁵³ and Vecchione et al.⁵² The list of genes generated in this analysis is in Table S3.

B cell receptor sequence processing and analysis

BCRs were obtained from 10X Genomics scRNASeq and processed using the Immcantation suite v4.5.0 (immcantation.org). BCR sequence data analysis began with the filtered V(D)J contigs from 10X Genomics Cell Ranger. To obtain initial V and J gene assignments, these contigs were aligned to the IMGT GENE-DB mouse germline reference allele database obtained Jan 25 2024⁷⁵ using IgBlast v1.22.0⁷⁶ and Change-O v1.3.0.⁷⁷ Non-productive heavy and light chain BCR sequences were removed. Only BCRs with CDRH3 lengths of 39 nucleotides and IMGT-gapped heavy chain sequence lengths of 385 nucleotides were retained, as well as IMGT-gapped light chains with lengths of 370nt. These lengths were chosen based on the CDRH3 and IMGT-gapped sequence lengths of the known heavy and light chain knock-in germlines,⁵ and 98.2% of cells were retained based on these length-filtering criteria. Remaining cells with multiple heavy chains (n=26, 0.4%) were also removed. For cells with multiple light chains (n=37, 0.7%), only the light chain with the highest UMI count was retained. One T to A mutation at site 85 of IMGT-gapped heavy chain nucleotide sequence was found at suspiciously high frequency (97.1% of cells, compared to the next most frequent at 46.8%) and presumed to be a mistake in the germline sequence. This site was changed from T to A in the germline. Cells were annotated by B cell subtype based on matching their single cell barcodes to the gene expression information.⁷⁶ Only cells that had both gene expression and BCR sequence data were retained for BCR analysis. SHM level was determined. Previously reported high affinity amino acid substitutions were quantified at CDRH3 amino acid positions 1, 5, 9, and 12 (IMGT amino acid positions 105, 109, 113, and 116).

QUANTIFICATION AND STATISTICAL ANALYSIS

Statistical information, including n (number of mice or cells per group), number of replicates, mean (center bars) and statistical significance values, are indicated in the figure legends. Normality was assessed using the Shapiro-Wilk test. Statistical significance was determined with GraphPad Prism v8.3.0 using the tests indicated in each figure.